Check for updates

Received: 28 April 2025 | Revised: 18 June 2025 | Accepted: 16 July 2025

DOI: 10.1002/zamm.70152

ORIGINAL PAPER

Analysis of the contact problem functionally graded layer placed on a Pasternak foundation

Aleyna Yazıcıoğlu[1] | **Murat Yaylacı**[2,3,4] | **Dursun Murat Sekban**[5] | **Hamdi Kuleyin**[6] | **Ecren Uzun Yaylacı**[7] | **Ahmet Birinci**[8] | **Samy Refahy Mahmoud**[9]

[1]Department of Civil Engineering, Akdeniz University, Antalya, Turkey

[2]Department of Civil Engineering, Faculty of Engineering and Architecture, Recep Tayyip Erdogan University, Rize, Turkey

[3]Turgut Kıran Maritime Faculty, Recep Tayyip Erdogan University, Rize, Turkey

[4]Murat Yaylacı-Luzeri R&D Engineering Company, Rize, Turkey

[5]Department of Marine Engineering Operations, Karadeniz Technical University, Trabzon, Turkey

[6]Department of Mechanical Engineering, Recep Tayyip Erdogan University, Rize, Turkey

[7]Faculty of Fisheries, Recep Tayyip Erdogan University, Rize, Turkey

[8]Department of Civil Engineering, Karadeniz Technical University, Trabzon, Turkey

[9]GRC Department, Applied College, King Abdulaziz University, Jeddah, Saudi Arabia

Correspondence
Murat Yaylacı, Department of Civil Engineering, Faculty of Engineering and Architecture, Recep Tayyip Erdogan University, 53100, Rize, Turkey.
Email: murat.yaylaci@erdogan.edu.tr

This paper uses analytical and numerical methods to investigate the frictionless receding contact problem of two layers, one functionally graded (FG), loaded by a circular rigid block and resting on a Pasternak foundation. The upper layer loaded by the circular punch has homogeneous properties and contains a single shear modulus, while the shear modulus of the bottom layer is changed depending on an exponential function, making it an FG layer. In the solution, Poisson's ratios of both layers are assumed to be constant, and their weights are neglected. First, the overview of the topic, the existing studies in the literature, and the gaps in these studies are discussed. Then, an analytical solution is performed using the theory of elasticity and the Fourier integral transform techniques. The problem is modeled, and a numerical solution is obtained using the ANSYS package program based on the finite element method (FEM). Finally, the two methods are compared, and the results are presented using tables and graphs. Comparing analytical and numerical (FEM) solutions for the frictionless receding contact problem involving a FG layer resting on a Pasternak foundation is the main goal of this study.

1 | INTRODUCTION

Contact problems, commonly encountered in engineering and mechanics, examine situations in which two or more solid bodies interact with each other. These problems involve complex issues such as stress distributions, deformations, and analyses of frictional effects that occur in the areas where surfaces come into contact. Numerous researchers have

This is an open access article under the terms of the Creative Commons Attribution License, which permits use, distribution and reproduction in any medium, provided the original work is properly cited.
© 2025 The Author(s). ZAMM - Journal of Applied Mathematics and Mechanics published by Wiley-VCH GmbH.

investigated contact problems with different geometries and properties, and these studies have been continuously updated in parallel with the emergence of new material properties in recent times.

By creating the first analytical formulation for contact stresses between curved elastic bodies, Hertz [1] laid the groundwork for later studies in both theoretical and applied mechanics, laying the groundwork for contact mechanics. In order to solve a larger class of contact problems with intricate boundary conditions, Sneddon [2] later extended this framework by introducing integral transform techniques. In addition to forming the mathematical framework of contemporary contact mechanics, these seminal works also directly influenced the analytical strategy used in this investigation. Contact problems caused by compression of elastic layers resting on elastic or rigid foundations with different types of blocks have been investigated by various researchers [3–8]. In addition, contact problems caused by two layers with different mechanical properties and heights resting on foundations with various properties have also been addressed by researchers [9–11]. Toward the end of the 1990s, the idea of functionally graded materials (FGM) emerged to improve the deficiencies in existing materials. Numerous studies have examined the development of functionally graded (FG) layers, in which the modulus of elasticity changes with height [12–17]. Among these, the study by Giannakopoulos and Suresh [12] is particularly noteworthy for demonstrating how elastic property gradients can be analytically modeled in contact problems involving indentation. Their work laid the foundation for subsequent models, including the present study, which applies similar principles to layered systems on elastic foundations. Using the plane equations of elasticity and the Fourier integral transform techniques, the contact between the layer and the block, where the shear modulus changes gradually, is solved analytically [18–20]. For example, Rhimi et al. [19] analyzed axisymmetric contact between a FG layer and a homogeneous substrate, highlighting the influence of material gradation on stress distribution—an aspect extended here for layered systems on elastic foundation.

The continuous and discontinuous contact problem of elastic, homogeneous, and isotropic layers, resting on a Winkler foundation and subjected to an axially symmetric distributed load of a certain length, has been investigated [21]. The FGM form of the layer has been solved analytically under load through a rigid punch [22]. Various computational techniques, such as the finite element method (FEM) and artificial neural networks, have been used by researchers to solve contact problems. The frictionless contact problem of FG layers resting on various foundations has been solved using analytical methods, FEM, and a multilayer perceptron, which is an artificial neural network [23, 24]. In addition, the effect of the Pasternak foundation on contact problems has been little studied in the literature [25, 26].

The literature review shows that analytical solutions have been developed for numerous contact problems with different geometries and material properties. However, the review lacks the effect of the Pasternak foundation on the contact problem and in terms of comparing the solution methods. In order to show the precision and usefulness of both approaches, the goal of this study is to compare analytical and FEM solutions to the frictionless receding contact problem, which has received little attention in the literature and involves a FG layer resting on a Pasternak foundation. For this purpose, in this study, the contact problem of two layers, one FG, loaded by a circular rigid block, and resting on a Pasternak foundation, has been solved using both the analytical method and the FEM. In the first part, stress and displacement expressions for homogeneous and FG layers are obtained using the theory of elasticity and integral transformation techniques. Then, these expressions are solved by substituting boundary conditions, and a system of equations is obtained in which the contact stresses are unknown. Using the Gauss–Chebyshev integration formulation, this system of integral equations is transformed into algebraic equations, resulting in unknown contact lengths and contact stresses. In the second part, the FEM and its advantages are discussed, followed by the modeling of the problem geometry in ANSYS, a finite element-based program. Finally, the results obtained from both solutions are presented in tables and graphs. The results are discussed comparatively, and their advantages are analyzed.

2 | MATERIAL AND METHOD

2.1 | Analytical solution

In this section, the analytical solution of the problem of frictionless contact of two layers, one of which is FG, with Pasternak foundation is presented, and the theory of elasticity is utilized in the solution. The upper layer is homogeneous and has a constant shear modulus, while the lower layer has FG properties with its shear modulus varying along its height (Equation 1).

$$\mu_2\ (y) = \mu_0\, e^{\lambda y}\ \ (-h_2 \le y \le 0) \tag{1}$$

15214001, 2025, 8, Downloaded from https://onlinelibrary.wiley.com/doi/10.1002/zamm.70152 by Turkey Cochrane Evidence Aid, Wiley Online Library on [07/08/2025]. See the Terms and Conditions (https://onlinelibrary.wiley.com/terms-and-conditions) on Wiley Online Library for rules of use; OA articles are governed by the applicable Creative Commons License

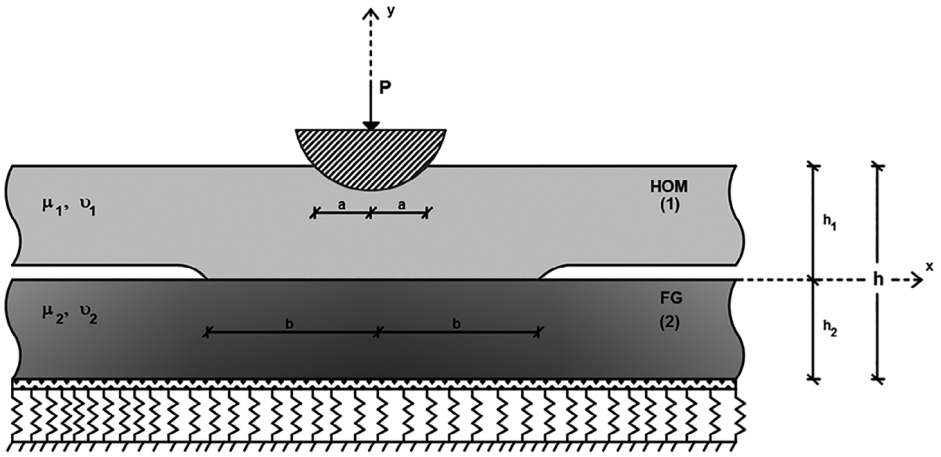


FIGURE 1 Geometry and loading of the contact problem.

In the equation, μ_0 represents the shear modulus at the upper surface of the FG layer, while λ denotes the stiffness parameter, given that it is a nonzero value. If λ is set to zero, the layer will transform into a homogeneous layer. The geometry and loading conditions of the problem are illustrated in Figure 1.

As shown in Figure 1, indices 1 and 2 represent the homogeneous (HOM) and FG layers, respectively. Here, the shear modulus $\mu_{1,2}$, Poisson's ratio $\upsilon_{1,2}$, and thicknesses $h_{1,2}$ of the layers are represented. The interval $(-a,+a)$ refers to the contact distance between the circular rigid block and the homogeneous layer, and the interval $(-b,+b)$ refers to the contact distance between the layers. It is assumed that the effect of gravitational force is neglected, contact between all surfaces is frictionless, and the thickness in the z-direction is taken as a unit.

Displacement and stress relations to be used in the solution of the problem are as follows for the HOM and FG layers.

For HOM layer displacement and stress expressions:

$$u_1\ (x,y) = \frac{2}{\pi}\int_0^\infty \left[(A_1 + A_2 y)\, e^{-\xi y} + (A_3 + A_4)\, e^{\xi y}\right] \sin(\xi x)\, d\xi \tag{2a}$$

$$v_1\ (x,y) = \frac{2}{\pi}\int_0^\infty \left\{\left[A_1 + \left(\frac{\kappa_1}{\xi} + y\right) A_2\right] e^{-\xi y} + \left[-A_3 + \left(\frac{\kappa_1}{\xi} - y\right) A_4\right] e^{\xi y}\right\} \cos(\xi x)\, d\xi \tag{2b}$$

$$\sigma_{x1}(x,y) = \frac{4\mu_1}{\pi}\int_0^\infty \left\{\left[\xi(A_1 + A_2 y) - \frac{3-\kappa_1}{2} A_2\right] e^{-\xi y} + \left[\xi(A_3 + A_4 y) + \frac{3-\kappa_1}{2} A_4\right] e^{\xi y}\right\} \cos(\xi x) d\xi \tag{3a}$$

$$\sigma_{y1}\ (x,y) = \frac{4\mu_1}{\pi}\int_0^\infty \left\{-\left[\xi(A_1 + A_2 y) + \frac{1+\kappa_1}{2} A_2\right] e^{-\xi y} + \left[-\xi(A_3 + A_4 y) + \frac{1+\kappa_1}{2} A_4\right] e^{\xi y}\right\} \cos(\xi x) d\xi \tag{3b}$$

$$\tau_{xy1}\ (x,y) = \frac{4\mu_1}{\pi}\int_0^\infty \left\{-\left[\xi(A_1 + A_2 y) + \frac{\kappa_1 - 1}{2} A_2\right] e^{-\xi y} + \left[\xi(A_3 + A_4 y) - \frac{\kappa_1 - 1}{2} A_4\right] e^{\xi y}\right\} \sin(\xi x) d\xi \tag{3c}$$

For FG layer displacement and stress expressions:

$$u_2\ (x,y) = \frac{2}{\pi}\int_0^\infty \sum_{j=1}^{4} B_j e^{n_j y} \sin(\xi x)\, d\xi \tag{4a}$$

$$v_2\ (x,y) = \frac{2}{\pi}\int_0^\infty \sum_{j=1}^{4} B_j m_j e^{n_j y} \cos(\xi x)\, d\xi \tag{4b}$$

$$\sigma_{x2}\ (x,y) = \frac{2\mu_2(y)}{\pi(\kappa_2 - 1)}\int_0^\infty \sum_{j=1}^{4} B_j \left[(\kappa_2 + 1)\xi + (3-\kappa_2) m_j n_j\right] e^{n_j y} \cos(\xi x) d\xi \tag{5a}$$

15214001, 2025, 8, Downloaded from https://onlinelibrary.wiley.com/doi/10.1002/zamm.70152 by Turkey Cochrane Evidence Aid, Wiley Online Library on [07/08/2025]. See the Terms and Conditions (https://onlinelibrary.wiley.com/terms-and-conditions) on Wiley Online Library for rules of use; OA articles are governed by the applicable Creative Commons License

$$\sigma_{y2}\ (x,y) = \frac{2\mu_2\,(y)}{\pi\,(\kappa_2-1)} \int_0^{\infty} \sum_{j=1}^{4} B_j C_j e^{n_j y} \cos(\xi x) d\xi \tag{5b}$$

$$\tau_{xy2}\ (x,y) = \frac{2\mu_2\,(y)}{\pi} \int_0^{\infty} \sum_{j=1}^{4} B_j D_j e^{n_j y} \sin(\xi x) d\xi \tag{5c}$$

where $u_i(x,y)$ and $v_i(x,y)$ are the components of the displacement vector, and $\sigma_{xi}(x,y)$, $\sigma_{yi}(x,y)$ and $\tau_{xyi}(x,y)$ (for $i=1,2$) are the stress components of the layers. It is known that the value of the Kolosov constant for the plane strain state is given by $\kappa_i = (3-4\upsilon_i)$ and υ_i is the Poisson's ratio. Given in the appendix m_j, n_j, C_j and D_j (for $j=1,2,3,4$) are the characteristic equation, the roots of the characteristic equation, and the known functions, respectively. A_j and B_j are the unknown coefficients for the layers that are determined from the boundary conditions of the problem. The boundary conditions for the problem are as follows:

Boundary conditions:

$$\sigma_{y1}\ (x,h_1) = \left\{ \begin{matrix} -p_1\,(x);\ (0 \le x < a) \\ 0;\ (a \le x < \infty) \end{matrix} \right\} \tag{6a}$$

$$\tau_{xy1}\ (x,h_1) = 0,\ (0 \le x < \infty) \tag{6b}$$

$$\sigma_{y2}\ (x,0) = \left\{ \begin{matrix} -p_2\,(x);\ (0 \le x < b) \\ 0;\ (b \le x < \infty) \end{matrix} \right\} \tag{6c}$$

$$\sigma_{y1}\ (x,0) = \sigma_{y2}\ (x,0),\ (0 \le x < \infty) \tag{6d}$$

$$\tau_{xy1}\ (x,0) = 0,\ (0 \le x < \infty) \tag{6e}$$

$$\tau_{xy2}\ (x,0) = 0,\ (0 \le x < \infty) \tag{6f}$$

$$\sigma_{y2}\ (x,-h_2) = k_w\,\upsilon_2\,(x,-h_2) - k_p \frac{\partial^2 \upsilon_2\,(x,-h_2)}{\partial x^2},\ (0 \le x < \infty) \tag{6g}$$

$$\tau_{xy2}\ (x,-h_2) = 0,\ (0 \le x < \infty) \tag{6h}$$

$$\frac{\partial}{\partial x}\ [\upsilon_1\,(x,h_1)] = \frac{\partial F\,(x)}{\partial x},\ (0 \le x < a) \tag{7a}$$

$$\frac{\partial}{\partial x}\ [\upsilon_1\,(x,0) - \upsilon_2\,(x,0)] = 0,\ (0 \le x < b) \tag{7b}$$

Equilibrium conditions of the problem can be expressed as:

$$\int_{-a}^{a} p_1\,(x)\,dx = P, \quad \int_{-b}^{b} p_2\,(x)\,dx = P \tag{8}$$

In the above boundary conditions and equilibrium equations, $p_1(x)$ is the unknown expressing the contact stresses between the HOM and the circular rigid block, $p_2(x)$ is the unknowns expressing the contact stresses between the HOM and the FG layer. P, k_w, k_p and $F(x)$ represent, respectively, the applied point load through the circular rigid block, the dimensionless spring constant and shear modulus related to the Pasternak foundation and the function related to the

15214001, 2025, 8, Downloaded from https://onlinelibrary.wiley.com/doi/10.1002/zamm.70152 by Turkey Cochrane Evidence Aid, Wiley Online Library on [07/08/2025]. See the Terms and Conditions (https://onlinelibrary.wiley.com/terms-and-conditions) on Wiley Online Library for rules of use; OA articles are governed by the applicable Creative Commons License

profile of the circular rigid block. These symbols are defined as follows:

$$F\ (x) = \left[\left(R^2 - x^2\right)^{0.5} - R\right] \tag{9a}$$

$$k/\ \mu_0 = k_w \tag{9b}$$

$$G\ /\ \mu_0 = k_p \tag{9c}$$

Using the stress components (Equations 3–5) and boundary conditions (Equation 6), the coefficients A_j and B_j are obtained based on the unknown contact stresses. These expressions are available in the appendix. To obtain the unknown contact stresses $p_1(x)$ and $p_2(x)$, displacement expressions (Equations 2–4) and the boundary condition (7) are used, and after some routine manipulations, a system of two integral equations is derived.

$$\frac{2}{\pi}\int_{-a}^{a} p_1(t_1)\left\{V_1(x_1,\ t_1) - \frac{\kappa_1+1}{8\mu_1}\left[\frac{1}{t_1 - x_1}\right]\right\} dt_1 + \frac{2}{\pi}\int_{-b}^{b} p_2(t_2)\, V_2(x_1,\ t_2)\, d\, t_2 = \frac{X}{R} \tag{10a}$$

$$\frac{2}{\pi}\int_{-a}^{a} p_1(t_1)\, Z_1(x_2,\ t_1)\, dt_1 + \frac{2}{\pi}\int_{-b}^{b} p_2(t_2)\{Z_2(x_2,\ t_2) - Z_3(x_2,\ t_2) + \left(\frac{\kappa_1+1}{8\mu_1} + \frac{\kappa_2+1}{8\mu_0}\right)\left(\frac{1}{t_2 - x_2}\right)\Big\}\, d\, t_2 = 0 \tag{10b}$$

where $V_1, V_2,\ Z_1,\ Z_2$, and Z_3 are described in Appendix.

The numerical solution of the integral equations will be carried out using the Gauss–Jacobi integration formulation. For this, dimensionless quantities can be defined using the following transformations of variables.

$$x_1 = as_1\ x_2 = bs_2 \tag{11a}$$

$$t_1 = ar_1\ t_2 = br_2 \tag{11b}$$

$$dt_1 = adr_1\ dt_2 = bdr_2 \tag{11c}$$

$$\xi = z/h_1\ d\xi = dz/h_1 \tag{11d}$$

$$p_1\ (t_1) = \frac{P}{h_1}\, G_1(r_1) \tag{11e}$$

$$p_2\ (t_2) = \frac{P}{h_1}\, G_2(r_2) \tag{11f}$$

By substituting the dimensionless quantities given in (11) into (8) and (10), the equations can be rewritten as follows:

$$\int_{-1}^{1} G_1(r_1)\left\{\frac{a}{h_1}V_1^*(s_1,\ r_1) - \frac{\kappa_1+1}{8}\left[\frac{1}{r_1 - s_1}\right]\right\} dr_1 + \frac{b}{h_1}\int_{-1}^{1} G_2(r_2)\, V_2^*(s_1,\ r_2)\, d\, r_2 = \frac{\pi}{2}\,\frac{\mu_1}{P/h_1}\,\frac{a/h_1}{R/h_1}s_1 \tag{12a}$$

$$\frac{a}{h_1}\int_{-1}^{1} G_1(r_1)\, Z_1^*(s_2,\ r_1)\, dr_1 + \int_{-b}^{b} G_2(r_2)\left\{\frac{b}{h_1}Z_2^*(s_2,\ r_2) - \frac{b}{h_1}Z_3^*(s_2,\ r_2) + \left(\frac{\kappa_1+1}{8\mu_1} + \frac{\kappa_2+1}{8\mu_0}\right)\left(\frac{1}{r_2 - s_2}\right)\right\} d\, r_2 = 0 \tag{12b}$$

$$\frac{a}{h_1}\int_{-1}^{1} G_1(r_1)\, d\, r_1 = 1,\ \frac{b}{h_1}\int_{-1}^{1} G_2(r_2)\, d\, r_2 = 1 \tag{12c}$$

15214001, 2025, 8, Downloaded from https://onlinelibrary.wiley.com/doi/10.1002/zamm.70152 by Turkey Cochrane Evidence Aid, Wiley Online Library on [07/08/2025]. See the Terms and Conditions (https://onlinelibrary.wiley.com/terms-and-conditions) on Wiley Online Library for rules of use; OA articles are governed by the applicable Creative Commons License

The solution of a system of integral equations expressed dimensionless is given by the following formulas:

$$G_i\ (r_i) = w_i\ (r_i)\, g_i\,(r_i)\,,\ w_i\ (r_i) = (1-r_i)^{\alpha}(1+r_i)^{\beta_i}\quad (i=1,2) \tag{13}$$

Because of the smooth contact at the end points, a and b, the contact pressures, $p_1(x)$ and $p_2(x)$, are zero at the edges. Thus, Equation (13) has an index of −1, and the following expressions can be derived [27]:

$$G_i\ (r_i) = w_i\ (r_i)\, g_i\,(r_i)\,,\ w_i\ (r_i) = \left(1-r_i^2\right)^{0,5}\quad (i=1,2) \tag{14}$$

By substituting the expressions given in Equation (14) into Equation (12), the equations can be rewritten as follows:

$$\sum_{i=1}^{N} w_{1i} g_1\,(r_{1i}) \left\{ \frac{a}{h_1} V_1^*\,(s_{1k},\ r_{1i}) - \frac{\kappa_1+1}{8}\left[\frac{1}{r_{1i}-s_{1k}}\right]\right\} + \frac{b}{h_1}\ \sum_{i=1}^{N} w_{2i} g_2\,(r_{2i})\, V_2^*\,(s_{1k},\ r_{2i}) = \frac{\pi}{2}\ \frac{\mu_1}{P/h_1}\frac{a/h_1}{R/h_1} s_{1k} \tag{15a}$$

$$\frac{a}{h_1}\sum_{i=1}^{N} w_{1i} g_1\,(r_{1i})\, Z_1^*\,(s_{2k},\ r_{1i})$$

$$+\sum_{i=1}^{N} w_{2i} g_2\,(r_{2i}) \left\{ \frac{b}{h_1} Z_2^*\,(s_{2k},\ r_{2i}) - \frac{b}{h_1} Z_3^*\,(s_{2k},\ r_{2i})\ + \left(\frac{\kappa_1+1}{8\mu_1}+\frac{\kappa_2+1}{8\mu_0}\right)\left(\frac{1}{r_{2i}-s_{2k}}\right)\right\} = 0 \tag{15b}$$

$$\frac{a}{h_1}\ \sum_{i=1}^{N} w_{1i} g_1\,(r_{1i}) = 1,\ \frac{b}{h_1}\ \sum_{i=1}^{N} w_{2i} g_2\,(r_{2i}) = 1 \tag{15c}$$

where s_k and r_i are the roots of the related Jacobi polynomials and w_i^N is the weighting constant

$$s_k = \cos\left(\frac{\pi}{2}\frac{2k-1}{N+1}\right)\ ,\ (k=1,\ldots,N+1) \tag{16a}$$

$$r_i = \cos\left(\frac{i\pi}{N+1}\right)\ ,\ (i=1,\ldots,N) \tag{16b}$$

$$w_i^N = \pi\left(\frac{1-r_i^2}{N+1}\right)\ ,\ (i=1,\ldots,N) \tag{16c}$$

In the obtained system of linear equations, $g_1(r_{1i})$ and $g_2(r_{2i})$ the unknown contact stresses, are $2N+2$. Similarly, the system contains $2N+2$ linear equations. Thus, a system of linear equations consisting of $2N+2$ equations with $2N+2$ unknowns are obtained. The solution of this system of equations gives the unknown contact stresses and contact lengths. The equilibrium conditions given in Equation (15) must be satisfied by the obtained contact stresses and contact distances. Interpolation is performed iteratively until these conditions are met. After the equations are satisfied, the resulting contact stresses and contact lengths will represent the actual values.

2.2 | Finite element method

Contact mechanics examines the interactions of forces and deformations between surfaces in contact with each other. When the branch of mechanics is examined, it can be seen that studies have been conducted on the solution of contact mechanics problems. When the literature is examined, it is known that analytical methods, FEMs, experimental solutions, and artificial neural network methods are frequently used in solving contact mechanics problems [28–33]. On the other hand, due to its advantages, such as high compatibility with experimental results, applicability to complex geometries, flexibility in material selection, and changeability of loading conditions, solutions made with FEMs provide great advantages among these methods.

15214001, 2025, 8, Downloaded from https://onlinelibrary.wiley.com/doi/10.1002/zamm.70152 by Turkey Cochrane Evidence Aid, Wiley Online Library on [07/08/2025]. See the Terms and Conditions (https://onlinelibrary.wiley.com/terms-and-conditions) on Wiley Online Library for rules of use; OA articles are governed by the applicable Creative Commons License

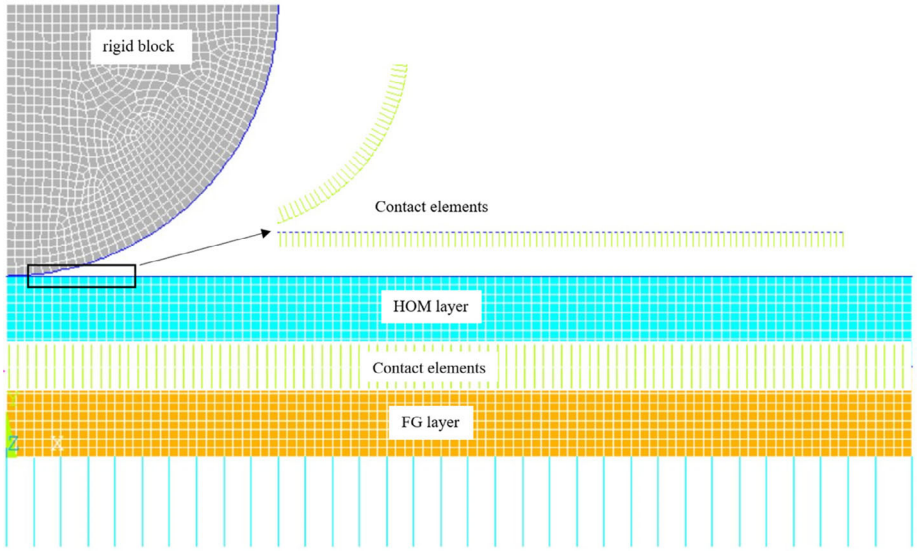


FIGURE 2 Mesh structure and contact elements.

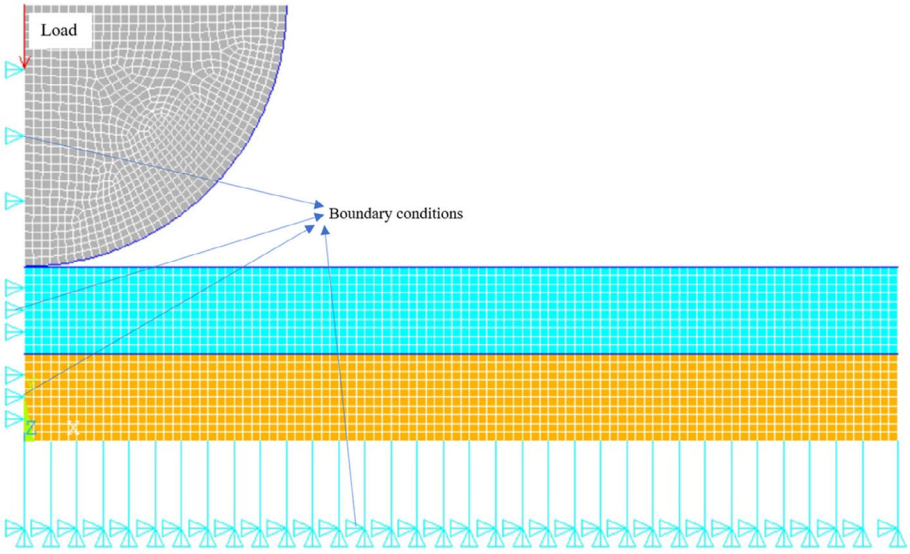


FIGURE 3 Boundary conditions and load.

FEM is a method used to mathematically model and solve the movements of physical systems. Considering the advantages we mentioned above, FEM analyses are also frequently used in the solutions of contact problems [34–43]. In this context, in this study, the contact problem modeled with FG material was solved with FEM using ANSYS software to obtain comparative results in addition to analytical solutions. In the first stage of FEM analysis, the geometry of the contact problem was determined, and the elements and material properties forming this geometry were assigned. In the contact problem modeled as two-dimensional plane stress, the initial dimension was reduced to an optimum dimension that would not affect the results, and the mesh structure was created using this dimension. The mesh structure used in the solution consists of 35,768 finite elements, 54,231 nodes, and 330 contact line elements. Preliminary experiments with various mesh densities were carried out before the mesh structure was finalized. After a certain mesh refinement level, the results showed very little variation, suggesting that the chosen mesh configuration produces stable and mesh-independent results. The contact elements and mesh structure used in the FEM model applied for the solution of the contact problem can be seen in Figure 2. Throughout the analysis, no numerical instabilities or convergence issues were encountered, as stable solver settings and sufficient mesh refinement were applied.

The boundary conditions and loadings used in the FEM model are shown in Figure 3. For the FEM analysis, the width and height of the layers were fixed with L/h1 = 50, and other required values were changed according to the analyses

15214001, 2025, 8, Downloaded from https://onlinelibrary.wiley.com/doi/10.1002/zamm.70152 by Turkey Cochrane Evidence Aid, Wiley Online Library on [07/08/2025]. See the Terms and Conditions (https://onlinelibrary.wiley.com/terms-and-conditions) on Wiley Online Library for rules of use; OA articles are governed by the applicable Creative Commons License

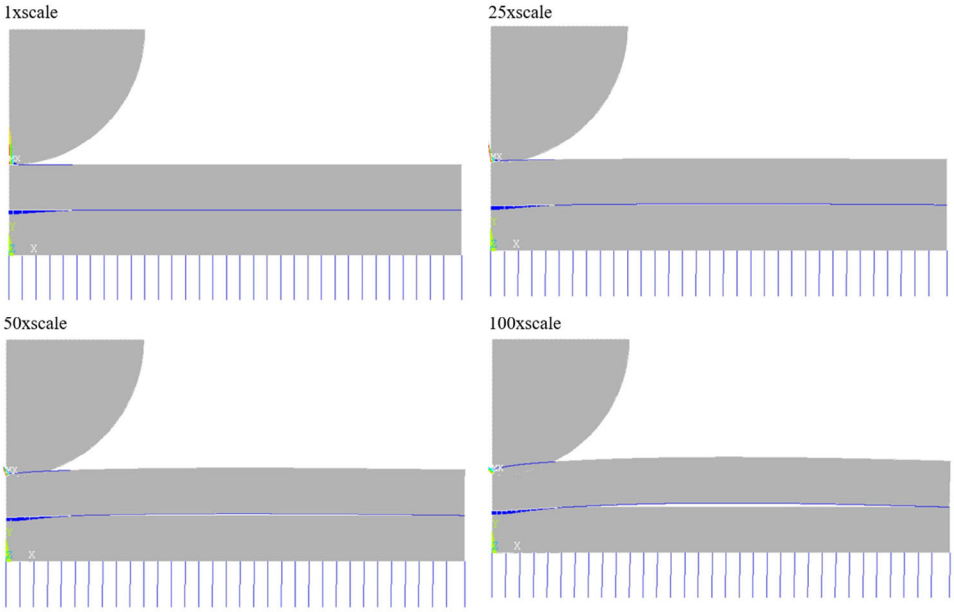


FIGURE 4 Deformed shape and contact stress of the problem.

performed. The FG layer's material characteristics are described as isotropic. The function Equation (1) $\mu_2(y) = \mu_0 e^{\lambda y}$ was used to calculate the shear modulus of the FG layer. Based on particular needs, the remaining solution parameters were chosen and modified as necessary.

The structural elements used in the FEM model were determined as PLANE 183 in the ANSYS program, which is defined as a non-rotating element consisting of eight nodes with two degrees of freedom assigned to each node. In addition, this element was allowed to move in the x and y directions and to be deformable. TARGE169 and CONTA172 elements were determined as contact pairs in the model, and analyses were performed under the determined boundary conditions and loadings by selecting the primary focal point as the elasticity value of the contacting surfaces. The deformations and stresses formed in the model after the FEM analyses can be seen in Figure 4.

3 | NUMERICAL RESULTS

This section presents the results obtained from analytical and numerical analyses considering the effects of stiffness parameter values, layer-to-height ratio, spring constant, Pasternak soil shear modulus, and shear modulus ratios of the layers on the contact stresses and contact lengths. The contact problem was analyzed and examined using both the analytical technique based on the theory of elasticity and the numerical method based on finite element modeling. where e, X_{ET} and X_{FEM} corresponds to the relative error percentile, analytical value, and FEM value obtained from solutions for the contact lengths and contact pressures, respectively.

The contact lengths and contact pressures are obtained from analytical solutions and FEM analysis, considering the effects of stamp radius, shear modulus, height ratio of the layers, Pasternak foundation spring constant, and Pasternak shear modulus. The results obtained from analytical and FEM solutions are summarized in Tables 1–5 and Figures 5–12, respectively. In addition to tables and figures, to better interpret the obtained data, the contact pressures and lengths were examined with different dimensionless quantities such as β_1, h_1/h_2, μ_1/μ_0.

Table 1 shows the changes in the contact lengths a/h_1 and b/h_1 depending on the stamp radius (R/h_1) and stiffness parameter for the FG layer (β_1). As can be decided from the table, the contact lengths increase with the increasing in the stamp radius and FG layer stiffness. It was also determined that the relative error between analytical and FEM solutions for this condition varied between 1.25%–2.18%. Based on this, it can be said that the analytical and FEM solutions are in good agreement to a large extent. The contact pressure variations in contact surfaces between the rigid stamp and homogeneous layer and between homogeneous layer and FG layer are given in Figure 5, depending on the stiffness of FG layer and stamp radius. As can be seen in the figure, due to the increase in the contact lengths between the rigid stamp and the layer, with the increase in the stamp radius, contact pressures decrease. Also, with the increase in the radius of the rigid stamp, the

15214001, 2025, 8, Downloaded from https://onlinelibrary.wiley.com/doi/10.1002/zamm.70152 by Turkey Cochrane Evidence Aid, Wiley Online Library on [07/08/2025]. See the Terms and Conditions (https://onlinelibrary.wiley.com/terms-and-conditions) on Wiley Online Library for rules of use; OA articles are governed by the applicable Creative Commons License

TABLE 1 Obtained contact lengths for contact surfaces, both rigid stamp/homogeneous layer (a/h_1) and homogeneous layer/FG layer (b/h_1), depending on various stamp radius (R/h_1) ($k_w = k_p = 1$, $h_1/h_2 = 1$, $\kappa_1 = \kappa_2 = 2$, $\mu_1/\mu_0 = 1$).

	a/h_1								
	$R/h_1 = 10$			$R/h_1 = 50$			$R/h_1 = 100$		
Parameters	**ET**	**FEM**	**e (%)**	**ET**	**FEM**	**e (%)**	**ET**	**FEM**	**e (%)**
$\beta_1 = -1$	0.219854	0.2163	1.61	0.500749	0.4940	1.35	0.717755	0.7021	2.18
$\beta_1 = 0.01$	0.220851	0.2180	1.30	0.510805	0.5019	1.74	0.741781	0.7292	1.70
$\beta_1 = 1$	0.222252	0.2179	1.97	0.525736	0.5143	2.18	0.778251	0.7685	1.25
	b/h_1								
	$R/h_1 = 10$			$R/h_1 = 50$			$R/h_1 = 100$		
	ET	**FEM**	**e (%)**	**ET**	**FEM**	**e (%)**	**ET**	**FEM**	**e (%)**
$\beta_1 = -1$	1.251549	1.2280	1.88	1.323122	1.3027	1.54	1.413195	1.3885	1.75
$\beta_1 = 0.01$	1.332804	1.3117	1.58	1.397999	1.3777	1.45	1.485439	1.4627	1.53
$\beta_1 = 1$	1.437649	1.4187	1.32	1.496970	1.4673	1.98	1.584113	1.5629	1.34

Abbreviations: FG, functionally graded; FME, functionally graded materials.

TABLE 2 Obtained contact lengths for contact surfaces, both rigid stamp/homogeneous layer (a/h_1) and homogeneous layer/FG layer (b/h_1), depending on different shear modulus ratios (μ_1/μ_0) ($k_w = k_p = 1$, $h_1/h_2 = 1$, $\kappa_1 = \kappa_2 = 2$, $R/h_1 = 20$).

	a/h_1								
	$\mu_1/\mu_0 = 1$			$\mu_1/\mu_0 = 5$			$\mu_1/\mu_0 = 10$		
Parameters	**ET**	**FEM**	**e(%)**	**ET**	**FEM**	**e(%)**	**ET**	**FEM**	**e(%)**
$\beta_1 = -1$	0.312623	0.3080	1.48	0.140481	0.1388	1.21	0.098964	0.0972	1.74
$\beta_1 = 0.01$	0.315382	0.3107	1.49	0.140931	0.1386	1.65	0.099133	0.0970	2.19
$\beta_1 = 1$	0.319330	0.3153	1.25	0.141499	0.1383	2.28	0.099348	0.0986	0.72
	b/h_1								
	$\mu_1/\mu_0 = 1$			$\mu_1/\mu_0 = 5$			$\mu_1/\mu_0 = 10$		
	ET	**FEM**	**e(%)**	**ET**	**FEM**	**e(%)**	**ET**	**FEM**	**e(%)**
$\beta_1 = -1$	1.269190	1.2457	1.85	1.959161	1.9355	1.21	2.378954	2.3342	1.88
$\beta_1 = 0.01$	1.348468	1.3277	1.54	2.050513	2.0191	1.53	2.481791	2.4260	2.25
$\beta_1 = 1$	1.451335	1.4313	1.38	2.186269	2.1408	2.08	2.639031	2.6118	1.03

Abbreviations: FG, functionally graded; FME, functionally graded materials.

TABLE 3 Obtained contact lengths for contact surfaces, both rigid stamp/homogeneous layer (a/h_1) and homogeneous layer/FG layer (b/h_1), depending on height ratio of the layers (h_1/h_2) ($k_w = k_p = 1$, $\mu_1/\mu_0 = 1$, $\kappa_1 = \kappa_2 = 2$, $R/h_1 = 10$).

	a/h_1								
	$h_1/h_2 = 0.5$			$h_1/h_2 = 1$			$h_1/h_2 = 2$		
Parameters	**ET**	**FEM**	**e(%)**	**ET**	**FEM**	**e(%)**	**ET**	**FEM**	**e(%)**
$\beta_1 = -1$	0.219229	0.2225	1.48	0.219854	0.2225	1.21	0.220076	0.2239	1.74
$\beta_1 = 0.01$	0.220881	0.2242	1.49	0.220851	0.2243	1.55	0.220452	0.2253	2.19
$\beta_1 = 1$	0.224164	0.2270	1.25	0.222252	0.2269	2.08	0.220903	0.2229	0.92
	b/h_1								
	$h_1/h_2 = 0.5$			$h_1/h_2 = 1$			$h_1/h_2 = 2$		
	ET	**FEM**	**e(%)**	**ET**	**FEM**	**e(%)**	**ET**	**FEM**	**e(%)**
$\beta_1 = -1$	1.167801	1.1882	1.75	1.251549	1.2692	1.41	1.263036	1.2868	1.88
$\beta_1 = 0.01$	1.347160	1.3666	1.44	1.332804	1.3532	1.53	1.286194	1.3151	2.25
$\beta_1 = 1$	1.708948	1.7394	1.78	1.437649	1.4647	1.88	1.313936	1.3275	1.03

15214001, 2025, 8, Downloaded from https://onlinelibrary.wiley.com/doi/10.1002/zamm.70152 by Turkey Cochrane Evidence Aid, Wiley Online Library on [07/08/2025]. See the Terms and Conditions (https://onlinelibrary.wiley.com/terms-and-conditions) on Wiley Online Library for rules of use; OA articles are governed by the applicable Creative Commons License

TABLE 4 Obtained contact lengths for contact surfaces, both rigid stamp/homogeneous layer (a/h_1) and homogeneous layer/FG layer (b/h_1), depending on Pasternak foundation spring constant (k_p) ($k_w = 1, \mu_1/\mu_0 = 1, \kappa_1 = \kappa_2 = 2, R/h_1 = 10, h_1/h_2 = 1$).

	a/h_1								
	$k_P = 10$			$k_P = 100$			$k_P = \infty$		
Parameters	**ET**	**FEM**	**e(%)**	**ET**	**FEM**	**e(%)**	**ET**	**FEM**	**e (%)**
$\beta_1 = -1$	0.218959	0.2222	1.48	0.218741	0.2212	1.12	0.218709	0.2225	1.74
$\beta_1 = 0.01$	0.219914	0.2232	1.49	0.219693	0.2231	1.55	0.219661	0.2224	1.26
$\beta_1 = 1$	0.221352	0.2241	1.25	0.221142	0.2251	1.80	0.221111	0.2249	1.73
	b/h_1								
	$k_P = 10$			$k_P = 100$			$k_P = \infty$		
	ET	**FEM**	**e(%)**	**ET**	**FEM**	**e(%)**	**ET**	**FEM**	**e (%)**
$\beta_1 = -1$	1.127381	1.1440	1.47	1.097739	1.1180	1.85	1.093404	1.1101	1.53
$\beta_1 = 0.01$	1.209245	1.2288	1.62	1.179251	1.1972	1.52	1.174866	1.1917	1.43
$\beta_1 = 1$	1.327986	1.3462	1.37	1.300038	1.3189	1.45	1.295839	1.3167	1.61

Abbreviations: FG, functionally graded; FME, functionally graded materials.

TABLE 5 Obtained contact lengths for contact surfaces, both rigid stamp/homogeneous layer (a/h_1) and homogeneous layer/FG layer (b/h_1), depending on Pasternak foundation shear modulus (k_w) ($\mu_1/\mu_0 = 1, \kappa_1 = \kappa_2 = 2, R/h_1 = 10, h_1/h_2 = 1, \beta = 0.01$).

	a/h_1								
	$k_w = 1$			$k_w = 5$			$k_w = 10$		
Parameters	**ET**	**FEM**	**e(%)**	**ET**	**FEM**	**e(%)**	**ET**	**FEM**	**e(%)**
$k_p = 10$	0.219914	0.2163	1.65	0.219833	0.2167	1.41	0.219794	0.2167	1.41
$k_p = 100$	0.219693	0.2169	1.25	0.219689	0.2163	1.56	0.219687	0.2163	1.56
$k_p = \infty$	0.219661	0.2168	1.32	0.219661	0.2160	1.65	0.219661	0.2160	1.65
	b/h_1								
	$k_w = 1$			$k_w = 5$			$k_w = 10$		
	ET	**FEM**	**e(%)**	**ET**	**FEM**	**e(%)**	**ET**	**FEM**	**e(%)**
$k_p = 10$	1.209245	1.1883	1.73	1.196974	1.1775	1.63	1.191304	1.1728	1.55
$k_p = 100$	1.179251	1.1613	1.52	1.178665	1.1616	1.45	1.178266	1.1596	1.58
$k_p = \infty$	1.174866	1.1528	1.88	1.174865	1.1540	1.78	1.174868	1.1552	1.67

Abbreviations: FG, functionally graded; FME, functionally graded materials.

contact length between the homogeneous layer and the FG layer also increases. This increase causes a decrease in contact pressures. When the effects of the stiffness parameter on the contact length and pressure are examined in Table 1 and Figure 5, the increase in the stiffness parameter (β) of the FG layer leads to a slight increase in the contact lengths between the rigid stamp and the homogeneous layer. As a result, a decrease in maximum contact pressures was observed. A similar effect occurs when the stiffness parameter between the homogeneous layer and the FG layer increases; this also results in longer contact lengths and reduces the contact pressures. Additionally, it has been determined that as stiffness decreases, the contact lengths decrease while the minimum contact pressure increases.

Table 2 presents the values of the contact lengths depending on both the ratio of the homogeneous layer shear modulus to the FG layer shear modulus and the rigidity of the FG layer. In addition, Figure 6 shows the changes in the contact pressure distribution on the contact surfaces between the rigid stamp and the homogeneous layer and between the homogeneous layer and the FG layer for the same parameter effects. As can be easily seen from the table, with the increase in the stiffness parameter, the contact length between the rigid block and the homogeneous layer does not change significantly. In contrast, the contact length between the homogeneous layer and the FG layer increases significantly. Accordingly, it is observed that the contact pressure distribution between the rigid stamp and the homogeneous layer does not change significantly with the increase of β (Figure 6). However, the maximum contact pressures between the homogeneous layer and the FG layer decrease with the increase in the stiffness of the FG layer. In addition, with the increase in the shear modulus ratio, the contact distance between the rigid block and the homogeneous layer decreases, while the contact distance between the homogeneous layer and the FG layer increases. As the shear modulus ratio of the layers increases, the contact pressures increase because of the decrease in the contact lengths between the rigid stamp and the homogeneous layer. This occurs as a result of the increase in the stiffness of the homogeneous layer.

15214001, 2025, 8, Downloaded from https://onlinelibrary.wiley.com/doi/10.1002/zamm.70152 by Turkey Cochrane Evidence Aid, Wiley Online Library on [07/08/2025]. See the Terms and Conditions (https://onlinelibrary.wiley.com/terms-and-conditions) on Wiley Online Library for rules of use; OA articles are governed by the applicable Creative Commons License

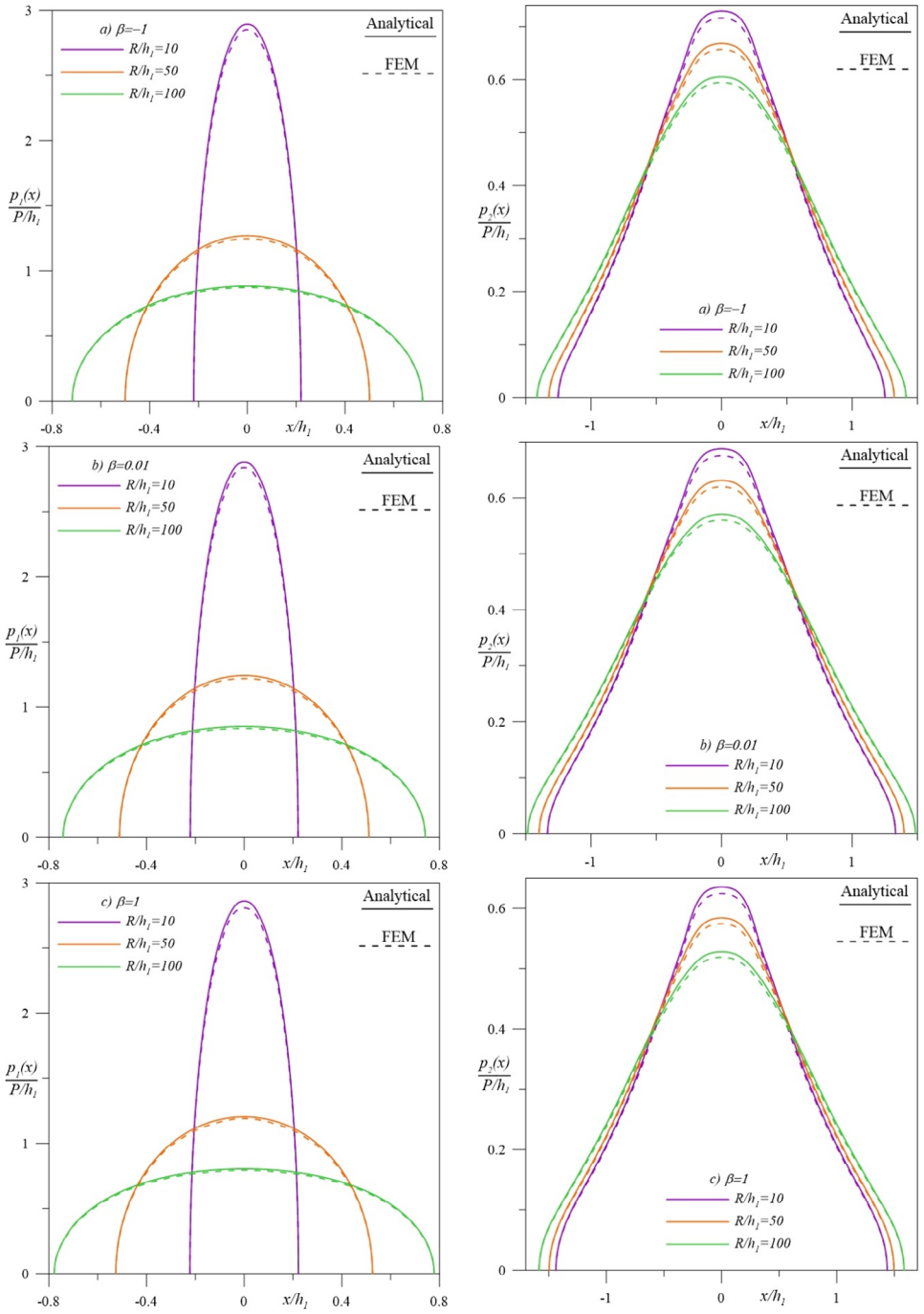


FIGURE 5 Contact pressure distribution in surfaces between rigid stamp and homogeneous layer and homogeneous layer and FG layer depending on stamp radius and stiffness of FG layer ($k_w = k_p = 1$, $h_1/h_2 = 1$, $\kappa_1 = \kappa_2 = 2$, $\mu_1/\mu_0 = 1$). FG, functionally graded.

The contact lengths data obtained from analytical and FEM solutions of the problem considering the effects of height ratios of homogenous layer to FG layer (h_1/h_2), and stiffness of the FG layer (β) given in Table 3. From Table 3, as the height ratio increases (h_1/h_2), the contact length between the rigid block and the homogeneous layer changes by a negligible degree, while the contact length between the homogeneous layer and the FG layer increases significantly. Similarly, it is seen that the contact lengths increase on both contact surfaces with the increase of β. In Figure 7, the variations of contact pressures along the contact surfaces between the rigid stamp and the homogeneous layer are given depending on height ratios and stiffness parameters. Similarly, Figure 8 presents the contact pressure distributions between the homogeneous layer and the FG layer. As can be understood from Figures 8 and 9, the minimum contact pressure values are obtained at the $h_1/h_2 = 1$ ratio on the contact surface between both the rigid stamp/homogeneous layer and the homogeneous layer/FG

15214001, 2025, 8, Downloaded from https://onlinelibrary.wiley.com/doi/10.1002/zamm.70152 by Turkey Cochrane Evidence Aid, Wiley Online Library on [07/08/2025]. See the Terms and Conditions (https://onlinelibrary.wiley.com/terms-and-conditions) on Wiley Online Library for rules of use; OA articles are governed by the applicable Creative Commons License

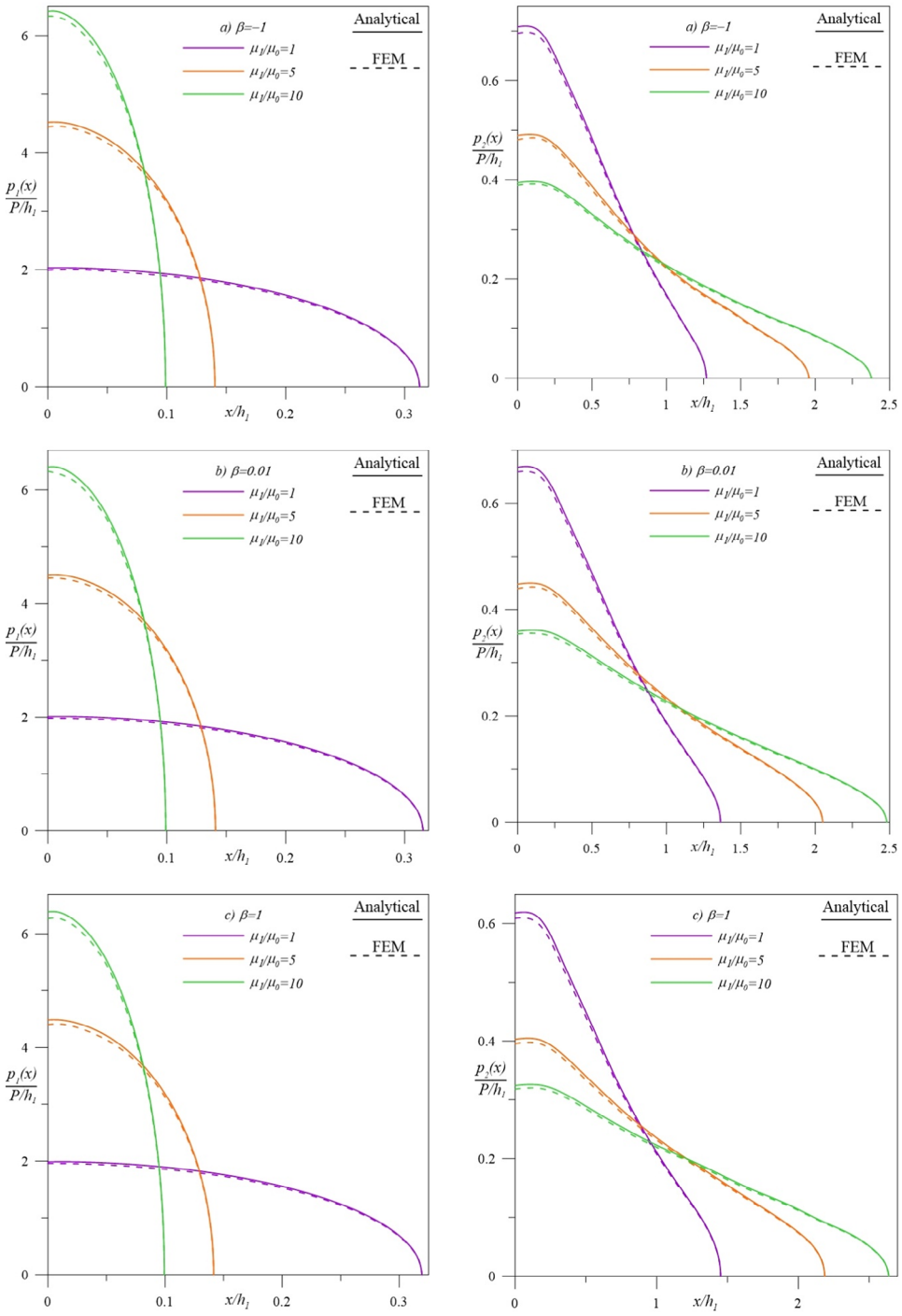


FIGURE 6 Contact pressure distribution in surfaces between rigid stamp and homogeneous layer and homogeneous layer and FG layer depending on shear modulus ratio and stiffness of FG layer ($k_w = k_p = 1$, $h_1/h_2 = 1$, $\varkappa_1 = \varkappa_2 = 2$, $R/h_1 = 20$). FG, functionally graded.

layer. Moreover, the change in the stiffness parameter does not cause a significant variation in the contact pressure value between the rigid block and the homogeneous layer. However, it is observed that it causes a significant effect on the contact pressure values between the homogeneous layer and the FG layer. It can be said that the contact pressure values decrease for different height ratios with the increase in the stiffness parameter of the FG layer.

The contact lengths value variations according to the Pasternak spring constant (k_p) and the stiffness of FG layer (β) obtained via ET and FEM solutions and presented in Table 4. In addition to this, the contact pressure distributions in the contact surfaces between the rigid stamp and homogeneous layer are shown in Figure 9. As the Pasternak foundation coefficient (k_p) increases, the vertical displacement of the foundation tends to decrease. Therefore, the foundation exhibits

15214001, 2025, 8, Downloaded from https://onlinelibrary.wiley.com/doi/10.1002/zamm.70152 by Turkey Cochrane Evidence Aid, Wiley Online Library on [07/08/2025]. See the Terms and Conditions (https://onlinelibrary.wiley.com/terms-and-conditions) on Wiley Online Library for rules of use; OA articles are governed by the applicable Creative Commons License

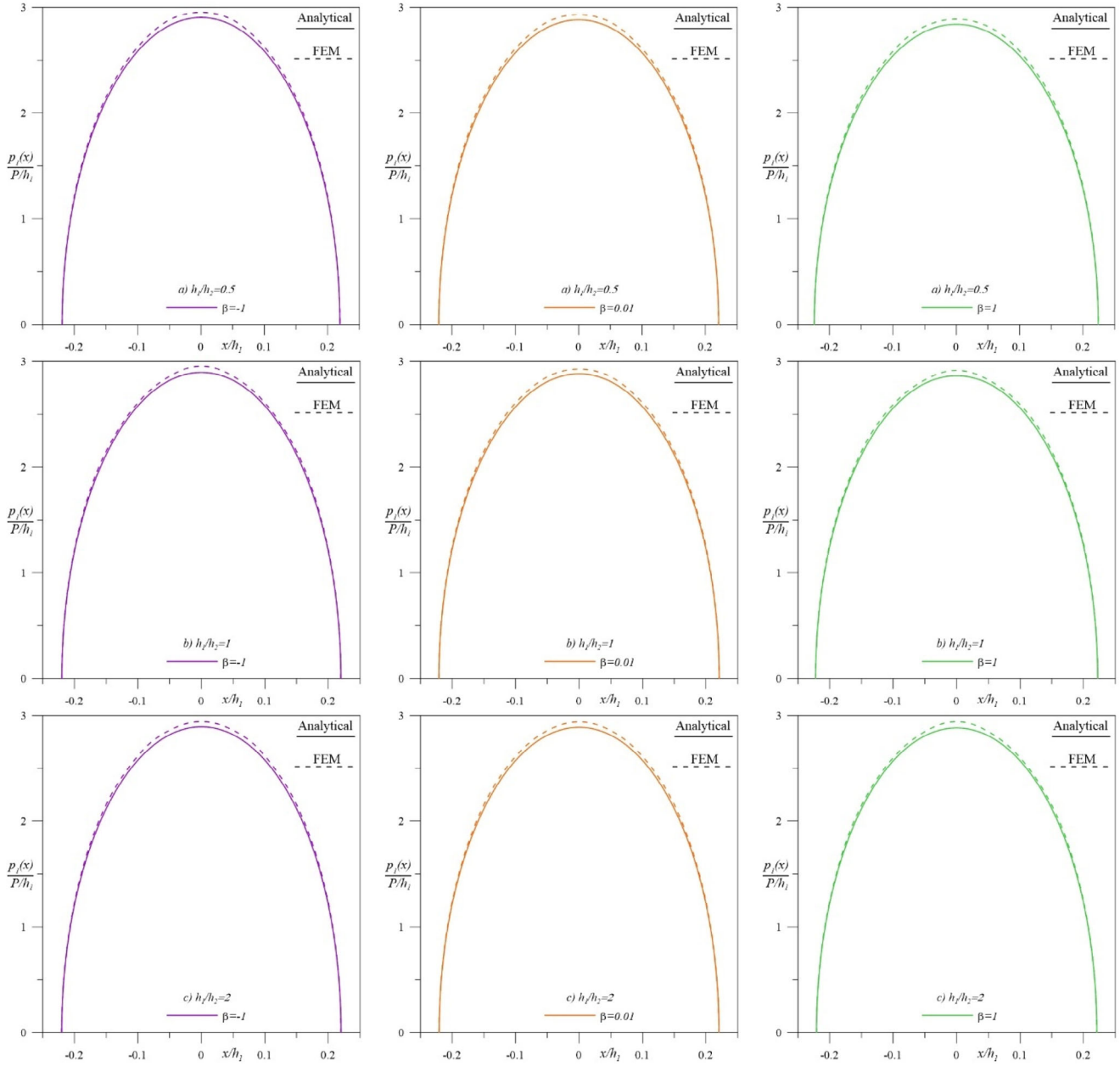


FIGURE 7 Contact pressure distribution in surfaces between rigid stamp and homogeneous layer depending on height ratio (h_1/h_2) of the layers and stiffness of FG layer (β) ($k_w = k_p = 1$, $\mu_1/\mu_0 = 1$, $\kappa_1 = \kappa_2 = 2$, $R/h_1 = 10$). FG, functionally graded.

more rigid behavior. It can be said that this situation leads to a decrease in the contact lengths between the foundation and the FG layer above it. There are no significant changes in the contact lengths and contact pressures between the rigid stamp and the homogeneous layer (Figure 9). The main reason for this situation is that the homogeneous layer is not in direct contact with the foundation. Additionally, similar results were obtained by increasing the stiffness of the FG layer. As can be seen from Table 4, as the value of k_p increases, the contact lengths for all stiffness values of the FG layer gradually decrease, and accordingly, the contact pressures increase for the homogenous layer/FG layer contact surface.

The contact lengths obtained from the analytical and numerical solutions of the problem, depending on both the Pasternak foundation spring constant and Pasternak foundation shear modulus values, are given in Table 5, respectively. When the table is examined, it is seen that there is no significant change in the contact lengths between the rigid stamp and the homogeneous layer. On the other hand, it can be said that the contact lengths between the homogeneous layer and the FG layer have decreased with an increase in the spring constant and shear modulus of the Pasternak foundation. The contact pressure variations in the contact surface between homogeneous layer and FG layer, depending on Pasternak spring con-

15214001, 2025, 8, Downloaded from https://onlinelibrary.wiley.com/doi/10.1002/zamm.70152 by Turkey Cochrane Evidence Aid, Wiley Online Library on [07/08/2025]. See the Terms and Conditions (https://onlinelibrary.wiley.com/terms-and-conditions) on Wiley Online Library for rules of use; OA articles are governed by the applicable Creative Commons License

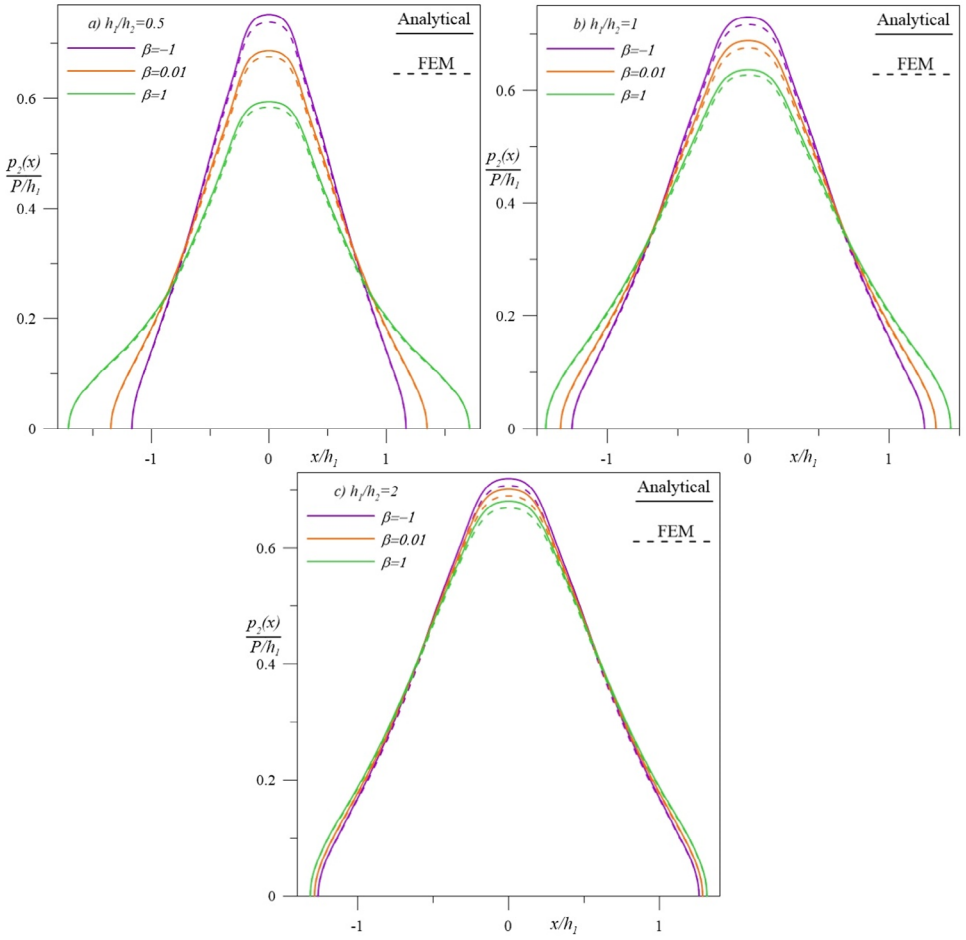


FIGURE 8 Contact pressure distribution in surface between homogeneous layer and FG layer depending on height ratio (h_1/h_2) of the layers and stiffness of FG layer (β) ($k_w = k_p = 1, \mu_1/\mu_0 = 1, \ \kappa_1 = \kappa_2 = 2, \ R/h_1 = 10$). FG, functionally graded.

stants, are presented in Figure 10. It can be said that with the increase of kp, the vertical displacement of the foundation will decrease, and therefore, the foundation will have a more rigid structure. In this case, the contact lengths between the homogeneous layer and the FG layer decrease, and the contact pressures increase. Similar effects are observed on the contact pressures in the case of a decrease in the stiffness of the FG layer.

The effects of Pasternak foundation shear modulus and stiffness of FG layer on contact pressure distribution between rigid stamp and homogeneous layer were examined with both analytical and FEM analysis. The results obtained from analysis, the contact pressure distribution between rigid stamp and homogeneous layer are given in Figure 11, according to the Pasternak foundation shear modulus and stiffness of FG layer. It is known that the contact lengths between the rigid stamp and homogeneous layer do not change significantly depending on the Pasternak foundation shear modulus and stiffness of FG layer values (Table 5). As a result of this, it is seen from the graphs given that, depending on both stiffness and Pasternak foundation shear modulus, there is no significant change in the contact pressures between the rigid stamp and the homogeneous layer. On the other hand, the contact pressure distribution between the homogeneous layer and FG layer is obtained with analytical and numerical solutions and given in Figure 8 depending on Pasternak foundation shear modulus and stiffness of FG layer. As can be seen from Table 5 and Figure 12, as the value of k_w increases, the contact lengths gradually decrease, and accordingly, the contact pressures increase in the contact surface between the homogeneous layer and the FG layer. Also, it is seen from Figure 12 that with the increase in the stiffness of the FG layer, the contact pressures decrease for homogeneous layer/FG layer contact surface.

Root mean square error (RMSE) and coefficient of determination (R^2) were used to evaluate the compatibility of analytical and FEM results. RMSE and R^2 were used to evaluate the compatibility of analytical and FEM results. The results obtained are shown in Table 6. The RMSE values approaching 0 indicate that the numerical results and analytical results

15214001, 2025, 8, Downloaded from https://onlinelibrary.wiley.com/doi/10.1002/zamm.70152 by Turkey Cochrane Evidence Aid, Wiley Online Library on [07/08/2025]. See the Terms and Conditions (https://onlinelibrary.wiley.com/terms-and-conditions) on Wiley Online Library for rules of use; OA articles are governed by the applicable Creative Commons License

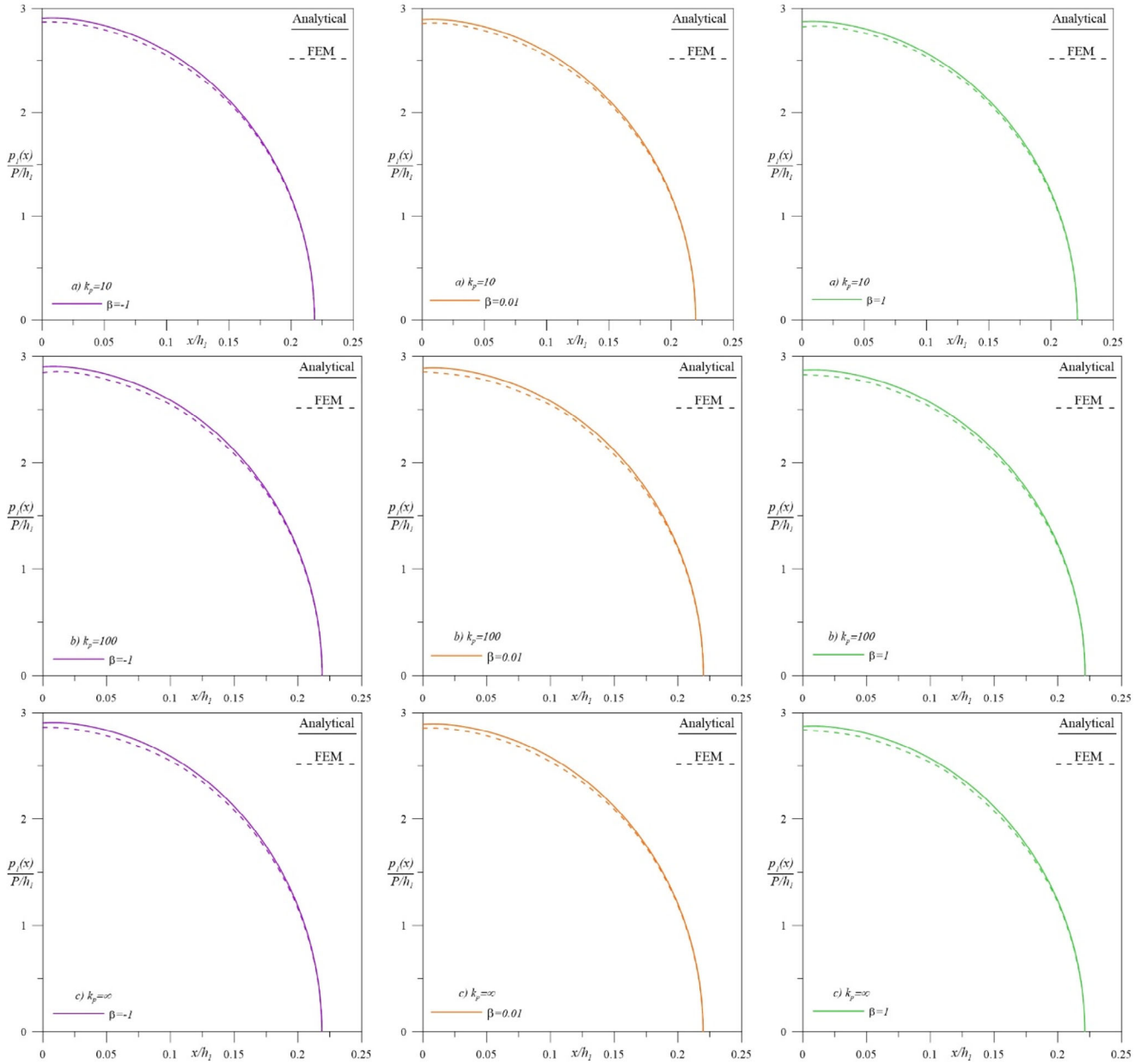


FIGURE 9 Contact pressure distribution in surface between rigid stamp and homogeneous layer depending on Pasternak spring constants (k_p) and stiffness of FG layer (β) ($k_w = 1, \mu_1/\mu_0 = 1, \ \kappa_1 = \kappa_2 = 2, \ R/h_1 = 10, h_1/h_2 = 1$). FG, functionally graded.

TABLE 6 E_{average}, $E_{\max}$, RMSE, and R^2 for contact pressures.

Figures	E_{average} %	$E_{\max}$ %	RMSE	R^2
Figure 5	1.54	1.88	0.01622	0.99999
Figure 6	1.57	1.85	0.03945	0.99999
Figure 7	1.61	1.96	0.03345	0.99997
Figure 8	1.54	1.92	0.00570	0.99999
Figure 9	1.50	1.89	0.03324	0.99999
Figure 10	1.58	1.82	0.00718	0.99998
Figure 11	1.55	1.96	0.03263	0.99997
Figure 12	1.57	1.87	0.00608	0.99999

Abbreviation: RMSE, root mean square error.

15214001, 2025, 8, Downloaded from https://onlinelibrary.wiley.com/doi/10.1002/zamm.70152 by Turkey Cochrane Evidence Aid, Wiley Online Library on [07/08/2025]. See the Terms and Conditions (https://onlinelibrary.wiley.com/terms-and-conditions) on Wiley Online Library for rules of use; OA articles are governed by the applicable Creative Commons License

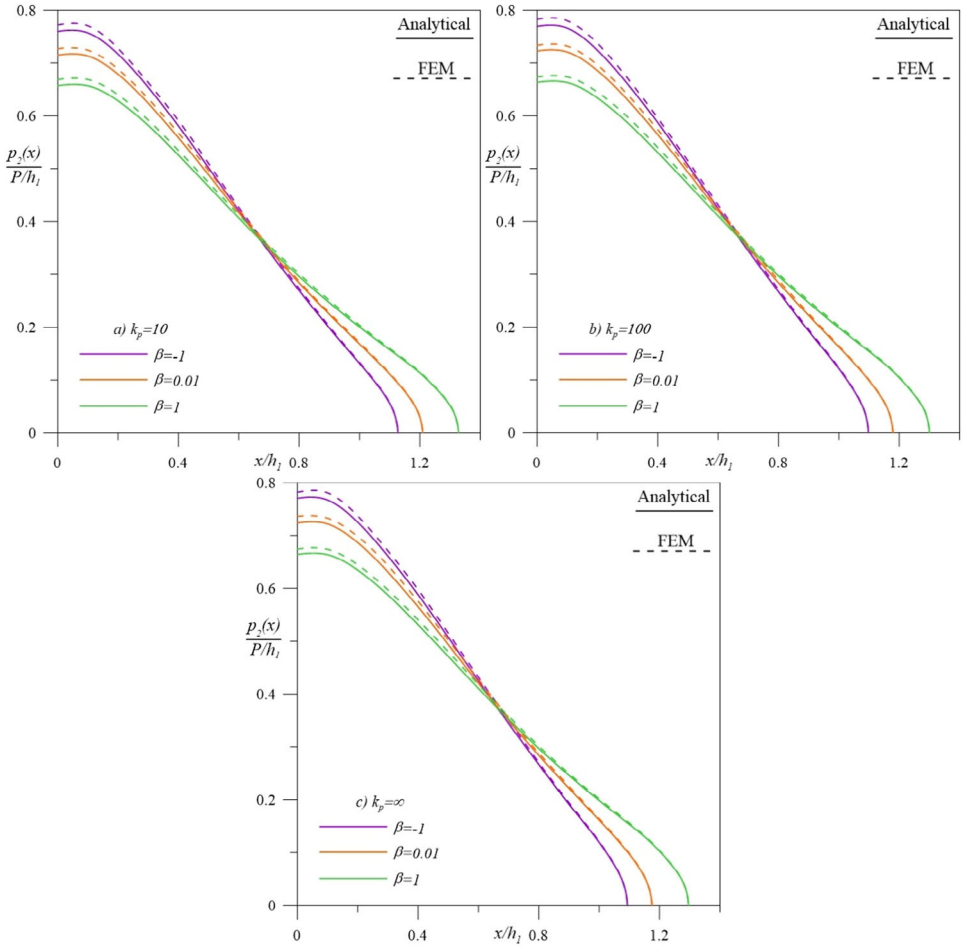


FIGURE 10 Contact pressure distribution in the surface between homogeneous layer and FG layer depending on Pasternak spring constants (k_p) and stiffness of FG layer (β) ($\mu_1/\mu_0 = 1,\ \kappa_1 = \kappa_2 = 2,\ R/h_1 = 10, h_1/h_2 = 1, \beta = 0.01$). FG, functionally graded.

are close to each other. The RMSE may be stated as the following [44]:

$$\mathrm{RMSE} = \sqrt{\frac{1}{n}\sum_{i}^{n}\left(R_{E_i} - R_{\mathrm{FEM}_i \mathrm{or} \mathrm{ANN}_i}\right)^2}, \qquad (i = 1, 2, 3, \ldots, n) \tag{17}$$

R^2 is the explanatory power of the model, and this value, being between 0.8 and 1, means that the solutions are consistent. The R^2 value is determined as follows [45]:

$$R^2 = 1 - \frac{\sum_i^n \left(R_{E_i} - R_{\mathrm{FEM}_i \mathrm{or} \mathrm{ANN}_i}\right)^2}{\sum_i^n \left(R_{E_i} - \overline{R}_E\right)^2}, \qquad (i = 1, 2, 3, \ldots, n) \tag{18}$$

Also, E_{average} in the table shows the average error percentage, while $E_{\max}$ shows the maximum error percentage. In addition, the amount of error between the two solution methods was also evaluated. For this purpose, the relative error, which is defined as the ratio of the convergence between the real value and the obtained value, was calculated by the following formulation [44]:

$$E\,(\%) = \left|\frac{X_{\mathrm{ET}} - X_{\mathrm{FEM}}}{X_{\mathrm{ET}}}\right| \times 100 \tag{19}$$

15214001, 2025, 8, Downloaded from https://onlinelibrary.wiley.com/doi/10.1002/zamm.70152 by Turkey Cochrane Evidence Aid, Wiley Online Library on [07/08/2025]. See the Terms and Conditions (https://onlinelibrary.wiley.com/terms-and-conditions) on Wiley Online Library for rules of use; OA articles are governed by the applicable Creative Commons License

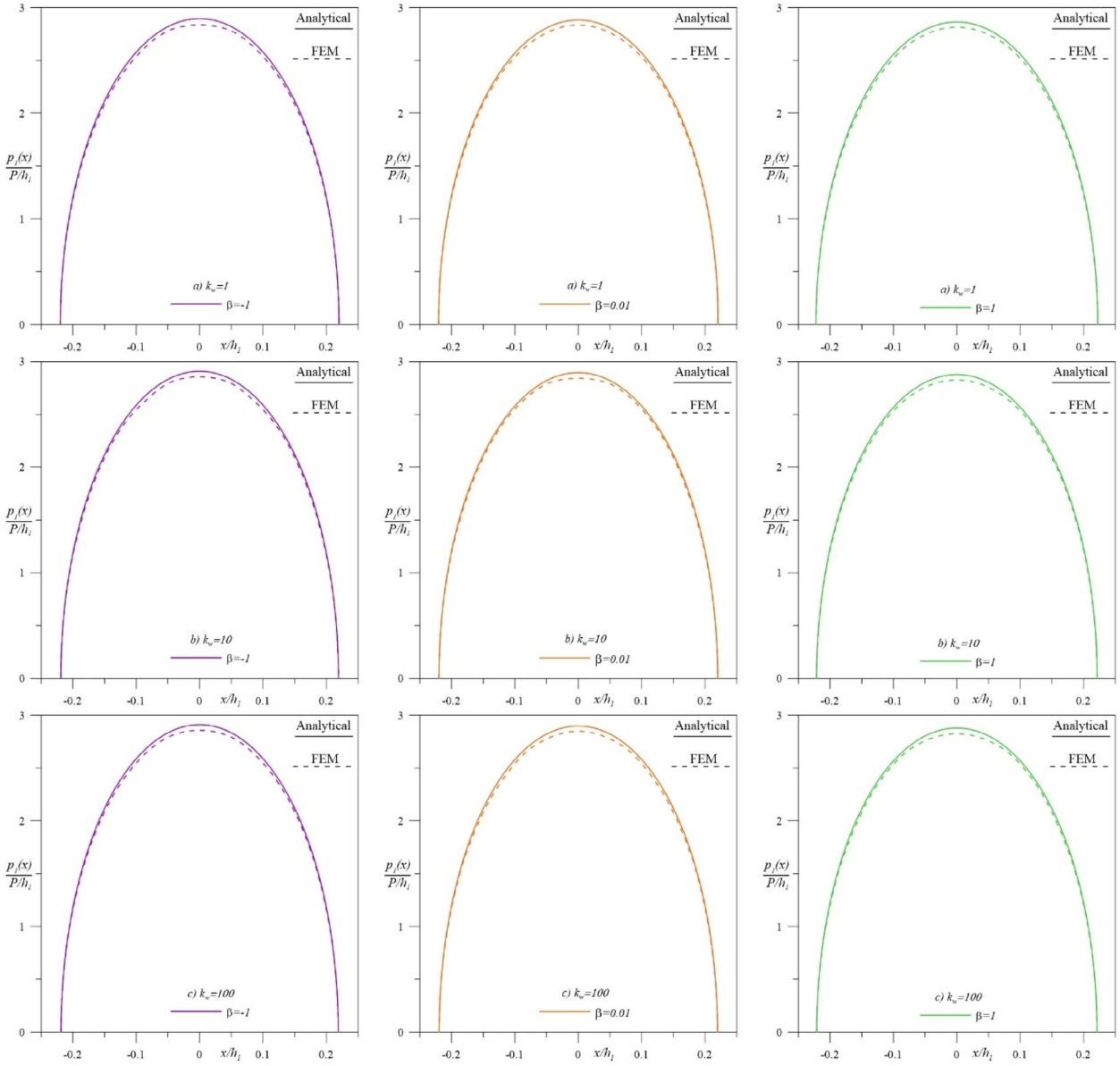


FIGURE 11 Contact pressure distribution in surface between rigid stamp and homogeneous layer depending on Pasternak spring constants (k_p) and stiffness of FG layer (β) ($\mu_1/\mu_0 = 1,\ \kappa_1 = \kappa_2 = 2,\ R/h_1 = 10, h_1/h_2 = 1, \beta = 0.01,\ k_p = 1$). FG, functionally graded.

The low E_{average} and $E_{\max}$ values obtained in Table 6, RMSE close to zero, and R^2 values very close to 1 show that the two methods give quite consistent results. These results clearly show the accuracy of the developed analytical model and that the FEM results are also in good agreement with the analytical results.

4 | CONCLUSIONS

This study investigates the frictionless receding contact problem of two FG layers, which are loaded by a circular rigid block and rest on a Pasternak foundation, using both analytical and numerical methods. The key findings from the study are given below:

1. The contact pressures between the homogeneous layer and the FG layer are dramatically reduced as the stiffness parameter of the FG layer increases, although the height ratio has a greater impact on the contact length than the contact pressure.

15214001, 2025, 8, Downloaded from https://onlinelibrary.wiley.com/doi/10.1002/zamm.70152 by Turkey Cochrane Evidence Aid, Wiley Online Library on [07/08/2025]. See the Terms and Conditions (https://onlinelibrary.wiley.com/terms-and-conditions) on Wiley Online Library for rules of use; OA articles are governed by the applicable Creative Commons License

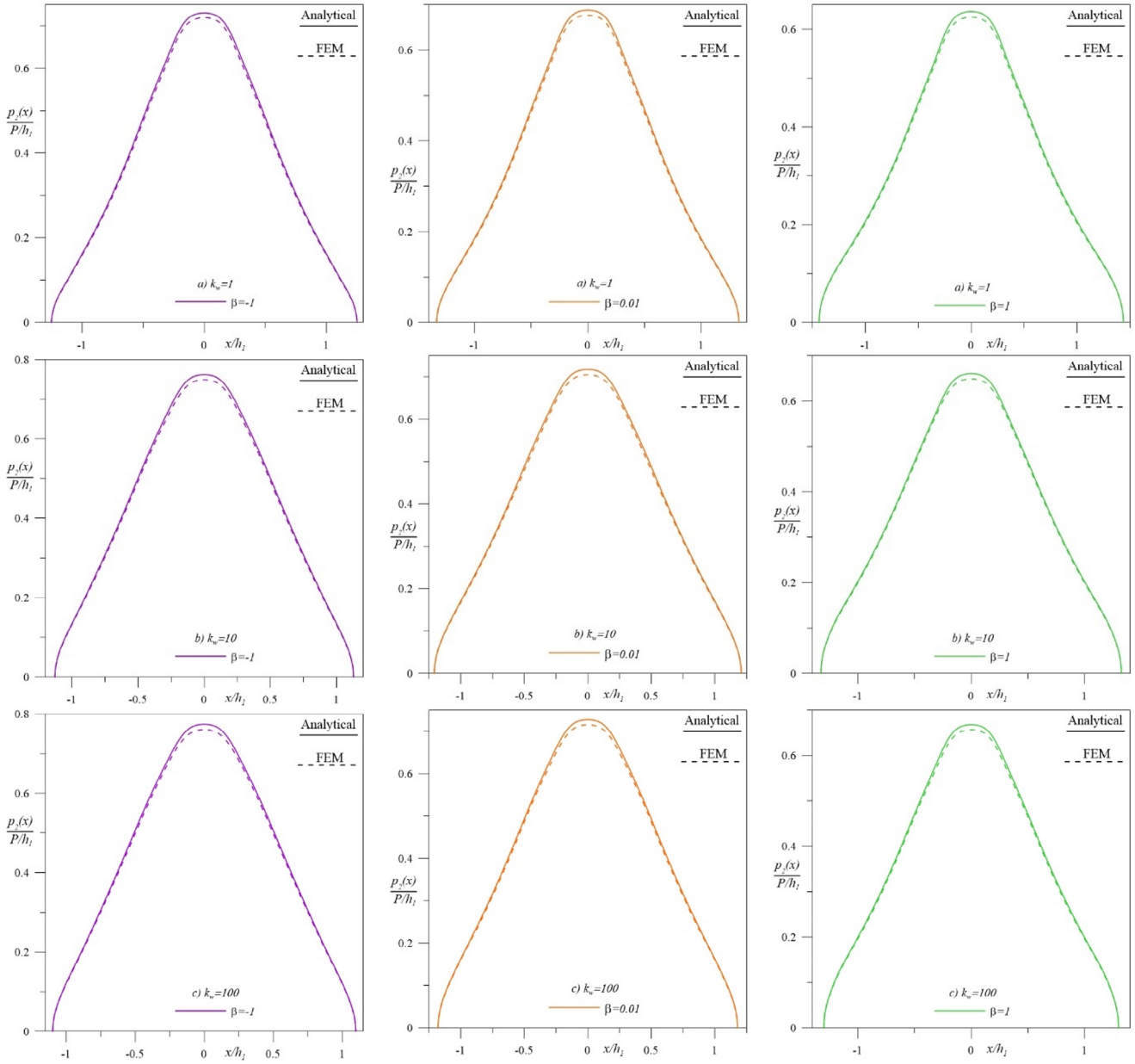


FIGURE 12 Contact pressure distribution in surface between rigid stamp and homogeneous layer depending on Pasternak spring constants (k_p) and stiffness of FG layer (β) ($\mu_1/\mu_0 = 1,\ \kappa_1 = \kappa_2 = 2,\ R/h_1 = 10, h_1/h_2 = 1, \beta = 0.01,\ k_p = 1$). FG, functionally graded.

2. Increases in the Pasternak foundation spring constant and shear modulus reduce contact length and increase contact pressure between the homogeneous and FG layers.
3. Although the contact lengths and the pressure distribution on the contact surface are only slightly affected by the Pasternak basic shear modulus and the stiffness of the FG layer, increasing the basic shear modulus at the homogeneous/FG layer interface reduces the contact length and raises the contact pressure, while the stiffness of the FG layer lowers this pressure.
4. Analytical and FEM findings showed strong agreement, with low RMSE values and R^2 values near 1.

The high agreement observed between the analytical and numerical results confirms the validity and robustness of the proposed model. Such contact models involving FG layers on elastic foundations are commonly encountered in engineering applications, particularly in civil engineering fields such as soil-structure interaction and pavement analysis, as well as in biomechanics, including joint mechanics and implant interface modeling. Even though the analytical and numerical

15214001, 2025, 8, Downloaded from https://onlinelibrary.wiley.com/doi/10.1002/zamm.70152 by Turkey Cochrane Evidence Aid, Wiley Online Library on [07/08/2025]. See the Terms and Conditions (https://onlinelibrary.wiley.com/terms-and-conditions) on Wiley Online Library for rules of use; OA articles are governed by the applicable Creative Commons License

results showed a high degree of agreement, it is important to keep in mind that this consistency may decline in more complicated configurations, such as when taking nonlinear foundation behavior, frictional contact, or material discontinuities into account. These elements could result in methodological differences and suggest possible lines of inquiry for further study. Additionally, the model may be extended in future studies to include three-dimensional configurations or dynamic loading scenarios to better reflect complex real-world conditions.

ACKNOWLEDGMENTS

The authors have nothing to report.

CONFLICT OF INTEREST STATEMENT

The authors declare that they have no known competing financial interests or personal relationships that could have appeared to influence the work reported in this paper.

DATA AVAILABILITY STATEMENT

The data that support the findings of this study are available on request from the corresponding author.

ORCID

Aleyna Yazıcıoğlu https://orcid.org/0009-0000-1794-5164
Murat Yaylacı https://orcid.org/0000-0003-0407-1685

REFERENCES

[1] Hertz, H.: Über die berührung fester elastischer körper. J. Reine Angew. Math. 92, 156–171 (1881).
[2] Sneddon, I. N.: Fourier Transforms. Mc. Grow-Hill Book Company, London (1951).
[3] King, R. B., O'sullivan, T. C.: Sliding contact stresses in a two-dimensional layered elastic half-space. Int. J. Solids Struct. 23, 581–597 (1987). https://doi.org/10.1016/0020-7683(87)90019-9
[4] Gecit, M. R.: A tensionless contact without friction between an elastic layer and an elastic foundation. Int. J. Solids Struct. 16, 387–396 (1980). https://doi.org/10.1016/0020-7683(80)90037-2
[5] Erdogan, F., Gupta, G. D.: The problem of an elastic stiffener bonded to a half plane. J. Appl. Mech. 38, 937–941 (1971). https://doi.org/10.1115/1.3408978
[6] Dhaliwal, R. S., Rau, I. S.: The axisymmetric Boussinesq problem for a thick elastic layer under a punch of arbitrary profile, Int. J. Eng. Sci., 8, 843–856 (1970). https://doi.org/10.1016/0020-7225(70)90086-8
[7] Alblas, J. B., Kuipers, M.: Contact problems of a rectangular block on an elastic layer of finite thickness: Part II: The thick layer, Acta Mech., 9, 1–12 (1970). https://doi.org/10.1007/BF01176605
[8] Adams, G. G.: An elastic strip pressed against an elastic half plane by a steadily moving force, J. Appl. Mech., 45, 89–94 (1978). https://doi.org/10.1115/1.3424279
[9] Çakıroğlu, F. L., Erdöl, R.: Elastik zemine oturan bileşik şeritte sürekli temas problemi, 6, Ulus. Mek. Kongr. Bild. Kıt., 1, 243–248 (1989).
[10] Kuo, C. H., Keer, L. M.: Contact stress analysis of a layered transversely isotropic half-space, J. Tribol., 114, 253–261 (1992). https://doi.org/10.1115/1.2920881
[11] Birinci, A., Erdol, R.: A frictionless contact problem for two elastic layers supported by a Winkler foundation, Struct. Eng. Mech., 15, 331–344 (2003).
[12] Giannakopoulos, A. E., Suresh, S.: Indentation of solids with gradients in elastic properties: Part II. Axisymmetric indentors, Int. J. Solids Struct., 34, 2393–2428 (1997). https://doi.org/10.1016/S0020-7683(96)00172-2
[13] Giannakopoulos, A. E., Pallot, P.: Two-dimensional contact analysis of elastic graded materials, J. Mech. Phys. Solids, 48, 1597–1631 (2000). https://doi.org/10.1016/S0022-5096(99)00068-X
[14] El-Borgi, S., Abdelmoula, R., Keer, L.: A receding contact plane problem between a functionally graded layer and a homogeneous substrate, Int. J. Solids Struct., 43, 658–674 (2006). https://doi.org/10.1016/j.ijsolstr.2005.04.017
[15] Ke, L. L., Wang, Y. S.: Two-dimensional contact mechanics of functionally graded materials with arbitrary spatial variations of material properties, Int. J. Solids Struct., 43, 18–19 (2006). https://doi.org/10.1016/j.ijsolstr.2005.06.081
[16] Liu, T. J., Wang, Y. S., Zhang, C.: Axisymmetric frictionless contact of functionally graded materials, Arch. Appl. Mech., 78, 267–282 (2008). https://doi.org/10.1007/S00419-007-0160-Y/METRICS
[17] Guler, M. A., Erdogan, F.: The frictional sliding contact problems of rigid parabolic and cylindrical stamps on graded coatings, Int. J. Mech. Sci., 49, 161–182 (2007). https://doi.org/10.1016/j.ijmecsci.2006.08.006
[18] Choi, H. J.: On the plane contact problem of a functionally graded elastic layer loaded by a frictional sliding flat punch, J. Mech. Sci. Technol., 23, 2703–2713 (2009). https://doi.org/10.1007/S12206-009-0734-4/METRICS
[19] Rhimi, M., El-Borgi, S., Ben Saïd, W., Jemaa, F. B: A receding contact axisymmetric problem between a functionally graded layer and a homogeneous substrate, Int. J. Solids Struct., 46, 3633–3642 (2009). https://doi.org/10.1016/j.ijsolstr.2009.06.008

15214001, 2025, 8, Downloaded from https://onlinelibrary.wiley.com/doi/10.1002/zamm.70152 by Turkey Cochrane Evidence Aid, Wiley Online Library on [07/08/2025]. See the Terms and Conditions (https://onlinelibrary.wiley.com/terms-and-conditions) on Wiley Online Library for rules of use; OA articles are governed by the applicable Creative Commons License

[20] Yan, J., Li, X.: Double receding contact plane problem between a functionally graded layer and an elastic layer, Eur. J. Mech. A/Solids, 53, 143–150 (2015). https://doi.org/10.1016/j.euromechsol.2015.04.001
[21] Birinci, A., Adıyaman, G., Yaylacı, M., Öner, E.: Analysis of continuous and discontinuous cases of a contact problem using analytical method and FEM, Lat. Am. J. Solids Struct., 12, 1771–1789 (2015). https://doi.org/10.1590/1679-78251574
[22] Adıyaman, G., Birinci, A.: A general solution for the receding contact problem of a functionally graded layer resting on a Winkler foundation, J. Struct. Eng. Appl. Mech., 1, 136–146 (2018). https://doi.org/10.31462/jseam.2018.03136146
[23] Yaylacı, M., Eyüboğlu, A., Adıyaman, G., Yaylacı, E. U., Öner, E., Birinci, A.: Assessment of different solution methods for receding contact problems in functionally graded layered mediums, Mech. Mater., 154, 103730 (2021). https://doi.org/10.1016/j.mechmat.2020.103730
[24] Öner, E., Şabano, B. Ş., Uzun Yaylacı, E., Adıyaman, G., Yaylacı, M., Birinci, A.: On the plane receding contact between two functionally graded layers using computational, finite element and artificial neural network methods. Z. Angew. Math. Mech. 102, e202100287 (2022). https://doi.org/10.1002/zamm.202100287
[25] Yazicioğlu, A., Birinci, A., Adiyaman, G.: A receding contact problem of two layers one of functionally graded, loaded by circular rigid block and resting on a Pasternak foundation, Turk. J. Civ. Eng., 35, 115–132 (2024). https://doi.org/10.18400/tjce.1392997
[26] Yaylacı, M., Yazıcıoğlu, A., Uzun Yaylacı, E., Terzi, M., Birinci, A.: Evaluation of the contact problem of two layers one of functionally graded, loaded by circular rigid block and resting on a Pasternak foundation by analytical and numerical (FEM and MLP) methods, Arch. Appl. Mech., 95, 78 (2025). https://doi.org/10.1007/s00419-025-02787-7
[27] Erdogan, F., Gupta, G. D.: On the numerical solution of singular integral equations, Q. Appl. Math. 29, 525–534 (1972). https://doi.org/10.1090/qam/408277
[28] Yaylacı, M., Yaylı, M., Öztürk, Ş., Ay, S., Özdemir, M. E., Uzun Yaylacı, E., Birinci, A.: Examining the contact problem of a functionally graded layer supported by an elastic half-plane with the analytical and numerical methods, Math. Methods Appl. Sci., 47, 10400–10420 (2024). https://doi.org/10.1002/mma.10129
[29] Öner, E., Uzun Yaylacı, E., Yaylacı, M.: Multi-method examination of contact mechanics in orthotropic layers under gravity, Mech. Mater. 195, 105036 (2024). https://doi.org/10.1016/j.mechmat.2024.105036
[30] Yaylacı, M., Öner, E., Adıyaman, G., Öztürk, Ş., Uzun Yaylacı, E., Birinci, A.: Analyzing of continuous and discontinuous contact problems of a functionally graded layer: Theory of elasticity and finite element method, Mech. Based Des. Struct. Mach. 52, 5720–5738 (2024). https://doi.org/10.1080/15397734.2023.2262562
[31] Aouadi, M.: A contact problem of a thermoelastic diffusion rod, Z. Angew. Math. Mech., 90(4), 278–286 (2010).
[32] Bock, I., Jarušek, J.: Dynamic contact problem for a von Kármán–Donnell shell, Z. Angew. Math. Mech., 93(10-11), 733–744 (2013).
[33] Miersemann, E.: On the measurement of surface tension and contact angle, Z. Angew. Math. Mech., 92(10), 824–828 (2012).
[34] Güvercin, Y., Yaylacı, M., Dizdar, A., Özdemir, M. E., Ay, S., Uzun Yaylacı, E., Karahasanoğlu, U., Uygun, H., Peker, G.: Biomechanical analysis and solution suggestions of screw replacement scenarios in femoral neck fracture surgeries: Finite element method, Orthop. Surg., 17, 614–623 (2025). https://doi.org/10.1111/os.14337
[35] Yemenoglu, H., Beder, M., Yaylacı, M., Dizdar, A., Alkurt, M., Naralan, M. E., Uzun Yaylacı, E., Özdemir, M. E., Öztürk, Ş., Yeşil, Z.: Evaluation of prostheses retained zygomatic and dental implants in large defects in the maxilla due to tumors or major trauma by biomechanical 3- dimensional finite element analysis. BMC Oral Health 25, 99 (2025). https://doi.org/10.1186/s12903-025-05468-7
[36] Yaylacı, M., Uzun Yaylacı, E., Turan, M., Özdemir, M. E., Öztürk, Ş., Ay, S.: Research of the crack problem of a functionally graded layer. Steel Compos. Struct. 50, 77–87 (2024). https://doi.org/10.12989/scs.2024.50.1.077
[37] Sekban, D. M., Uzun Yaylacı, E., Özdemir, M. E., Öztürk, Ş., Yaylacı, M., Panda, S. K.: Formability behavior of AH-32 shipbuilding steel strengthened by friction stir process, Theor. Appl. Fract. Mech. 132, 104485 (2024). https://doi.org/10.1016/j.tafmec.2024.104485
[38] Sekban, D. M., Uzun Yaylacı, E., Özdemir, M. E., Yaylacı, M.: Determination of formability behavior of steel used in ships by various methods, Struct. Eng. Mech., 92, 189–196 (2024). https://doi.org/10.12989/sem.2024.92.2.189
[39] Lefik, M., Boso, D. P., Schrefler, B. A.: Generalized self-consistent homogenization using the finite element method, Z. Angew. Math. Mech., 89(4), 306–319 (2009).
[40] Zeng, Y., Huang, P., He, Y.: Deferred defect-correction finite element method for the Darcy–Brinkman model, Z. Angew. Math. Mech., 101(11), e202000285 (2021).
[41] Freund, M., Ihlemann, J.: Generalization of one-dimensional material models for the finite element method, Z. Angew. Math. Mech., 90(5), 399–417 (2010).
[42] Barrenechea, G. R., Chouly, F.: A finite element method for the resolution of the reduced Navier–Stokes/Prandtl equations, Z. Angew. Math. Mech., 89(1) 54–68 (2009).
[43] Chen, Y., Hu, H.: Two-grid method for miscible displacement problem with dispersion by finite element method of characteristics, Z. Angew. Math. Mech., 101(3), e201900275 (2021).
[44] Chang, S., Arora, H. C., Kumar, A., Kontoni, D.-P. N., Kumar, P., Kapoor, N. R., Singh, J.: Estimation of confined compressive strength of LRS-FRP concrete specimens with computational intelligence, Z. Angew. Math. Mech., 104(10), e202400455 (2024).
[45] Tariq, A., Uzun, B., Deliktaş, B., Yaylı, M. Ö.: Assessment of machine learning methods predicting the axial vibration frequencies of microbars, Z. Angew. Math. Mech., 104(3), e202300916 (2024).

15214001, 2025, 8, Downloaded from https://onlinelibrary.wiley.com/doi/10.1002/zamm.70152 by Turkey Cochrane Evidence Aid, Wiley Online Library on [07/08/2025]. See the Terms and Conditions (https://onlinelibrary.wiley.com/terms-and-conditions) on Wiley Online Library for rules of use; OA articles are governed by the applicable Creative Commons License

How to cite this article: Yazıcıoğlu, A., Yaylacı, M., Sekban, D.M., Kuleyin, H., Yaylacı, E.U., Birinci, A., Mahmoud, S.R.: Analysis of the contact problem functionally graded layer placed on a Pasternak foundation. Z Angew Math Mech. 105, e70152 (2025). https://doi.org/10.1002/zamm.70152

APPENDIX

$$m_j = \frac{\left(3\beta + 2n_j - \beta\kappa_2\right)\left[n_j\left(\beta + n_j\right)\left(\kappa_2 + 1\right) - \xi^2\left(\kappa_2 + 3\right)\right]}{\xi\left[4\xi^2 - \beta^2\left(\kappa_2 - 3\right)\left(\kappa_2 + 1\right)\right]}, (j = 1, \ldots, 4)$$

$$n_1 = -\frac{1}{2}\left(\beta + \sqrt{4\xi^2 + \beta^2 - 4\xi\beta i\sqrt{\frac{3-\kappa_2}{\kappa_2+1}}}\right)$$

$$n_2 = -\frac{1}{2}\left(\beta - \sqrt{4\xi^2 + \beta^2 - 4\xi\beta i\sqrt{\frac{3-\kappa_2}{\kappa_2+1}}}\right)$$

$$n_3 = -\frac{1}{2}\left(\beta + \sqrt{4\xi^2 + \beta^2 + 4\xi\beta i\sqrt{\frac{3-\kappa_2}{\kappa_2+1}}}\right)$$

$$n_4 = -\frac{1}{2}\left(\beta - \sqrt{4\xi^2 + \beta^2 + 4\xi\beta i\sqrt{\frac{3-\kappa_2}{\kappa_2+1}}}\right)$$

$$C_j = \left[\left(\kappa_2 + 1\right)m_j n_j + \xi\left(3 - \kappa_2\right)\right] \quad (j = 1, 2, 3, 4)$$

$$D_j = \left[n_j - \xi m_j\right] \quad (j = 1, 2, 3, 4)$$

$$A_1 = \left\{\begin{array}{c} -p_1 e^{\xi h_1}\left[\kappa_1 + e^{2\xi h_1} + 2\xi h_1 - \kappa_1 e^{2\xi h_1} - 2\kappa_1\xi h_1 e^{2\xi h_1} - 1\right] \\ -p_2 e^{2\xi h_1}\left[1 - e^{2\xi h_1} - \kappa_1 + 4\xi^2 h_1^2 - 2\xi h_1 + \kappa_1 e^{2\xi h_1} + 2\xi\kappa_1 h_1\right] \end{array}\right\} / 4\mu_1\xi\Delta_1$$

$$A_2 = \left\{\begin{array}{c} -p_1 e^{\xi h_1}\left[e^{2\xi h_1} + 2\xi h_1 e^{2\xi h_1} - 1\right] \\ +p_2 e^{2\xi h_1}\left[e^{2\xi h_1} + 2\xi h_1 - 1\right] \end{array}\right\} / 2\mu_1\Delta_1$$

$$A_3 = \left\{\begin{array}{c} p_1 e^{\xi h_1}\left[\kappa_1 + e^{2\xi h_1} - \kappa_1 e^{2\xi h_1} - 2\kappa_1\xi h_1 + 2\xi h_1 e^{2\xi h_1} - 1\right] - p_2 \\ \left[e^{2\xi h_1} - 1 + \kappa_1 - \kappa_1 e^{2\xi h_1} + 4\xi^2 h_1^2 e^{2\xi h_1} + 2\xi h_1 e^{2\xi h_1} - 2\xi\kappa_1 h_1 e^{2\xi h_1}\right] \end{array}\right\} / 4\mu_1\xi\Delta_1$$

$$A_4 = \left\{\begin{array}{c} -p_1 e^{\xi h_1}\left[e^{2\xi h_1} + 2\xi h_1 - 1\right] \\ +p_2\left[e^{2\xi h_1} + 2\xi h_1 e^{2\xi h_1} - 1\right] \end{array}\right\} / 2\mu_1\Delta_1$$

15214001, 2025, 8, Downloaded from https://onlinelibrary.wiley.com/doi/10.1002/zamm.70152 by Turkey Cochrane Evidence Aid, Wiley Online Library on [07/08/2025]. See the Terms and Conditions (https://onlinelibrary.wiley.com/terms-and-conditions) on Wiley Online Library for rules of use; OA articles are governed by the applicable Creative Commons License

$$B_1 = \{-p_2(\kappa_2-1)e^{h_2 s_1}[\mu_0 e^{h_2 s_2}(C_3D_2D_4 - C_4D_2D_3) + \mu_0 e^{h_2 s_3}(C_4D_2D_3 - C_2D_3D_4)$$
$$+\mu_0 e^{h_2 s_4}(C_2D_3D_4 - C_3D_2D_4) + (e^{h_2(s_1+\beta)}(D_2D_4m_3 - D_2D_3m_4) + e^{h_2(s_1+\beta)}(D_2D_3m_4 - D_3D_4m_2)$$
$$+e^{h_2(s_1+\beta)}(D_3D_4m_2 - D_2D_4m_3))(1-\kappa_2)\left(k_w + \xi^2 k_p\right)]\}/\Delta_2$$

$$B_2 = \{-p_2(\kappa_2-1)e^{h_2 s_2}[\mu_0 e^{h_2 s_1}(C_3D_1D_4 - C_4D_1D_3) + \mu_0 e^{h_2 s_3}(C_4D_1D_3 - C_1D_3D_4)$$
$$+\mu_0 e^{h_2 s_4}(C_1D_3D_4 - C_3D_1D_4) + (e^{h_2(s_1+\beta)}(D_1D_4m_3 - D_1D_3m_4) + e^{h_2(s_3+\beta)}(D_1D_3m_4 - D_3D_4m_1)$$
$$+e^{h_2(s_4+\beta)}(D_3D_4m_1 - D_1D_4m_3))(1-\kappa_2)\left(k_w + \xi^2 k_p\right)]\}/\Delta_2$$

$$B_3 = \{-p_2(\kappa_2-1)e^{h_2 s_3}[\mu_0 e^{h_2 s_1}(C_2D_1D_4 - C_4D_1D_2) + \mu_0 e^{h_2 s_2}(C_4D_1D_2 - C_1D_2D_4)$$
$$+\mu_0 e^{h_2 s_4}(C_1D_2D_4 - C_2D_1D_4) + (e^{h_2(s_1+\beta)}(D_1D_4m_2 - D_1D_2m_4) + e^{h_2(s_2+\beta)}(D_1D_2m_4 - D_2D_4m_1)$$
$$+e^{h_2(s_4+\beta)}(D_2D_4m_1 - D_1D_4m_2))(1-\kappa_2)\left(k_w + \xi^2 k_p\right)]\}/\Delta_2$$

$$B_4 = \{-p_2(\kappa_2-1)e^{h_2 s_4}[\mu_0 e^{h_2 s_1}(C_2D_1D_3 - C_3D_1D_2) + \mu_0 e^{h_2 s_2}(C_3D_1D_2 - C_1D_2D_3)$$
$$+\mu_0 e^{h_2 s_3}(C_1D_2D_3 - C_2D_1D_3) + (e^{h_2(s_1+\beta)}(D_1D_3m_2 - D_1D_2m_3) + e^{h_2(s_2+\beta)}(D_1D_2m_3 - D_2D_3m_1)$$
$$+e^{h_2(s_4+\beta)}(D_2D_3m_1 - D_1D_3m_2))(1-\kappa_2)\left(k_w + \xi^2 k_p\right)]\}/\Delta_2$$

$$\Delta_1 = \left(1 - 2e^{2\xi h_1} + e^{4\xi h_1} - 4\xi^2 h_1^2 e^{2\xi h_1}\right)$$

$$\Delta_2 = \mu_0 \begin{bmatrix} (\mu_0)\left(e^{h_2(n_1+n_2)}(C_1C_3D_2D_4 - C_1C_4D_2D_3 - C_2C_3D_1D_4 + C_2C_4D_1D_3\right) \\ +e^{h_2(n_1+n_3)}(C_1C_4D_2D_3 - C_1C_2D_3D_4 - C_3C_4D_1D_2 + C_2C_3D_1D_4) \\ +e^{h_2(n_1+n_4)}(C_1C_2D_3D_4 - C_1C_3D_2D_4 - C_2C_4D_1D_3 + C_3C_4D_1D_2) \\ +e^{h_2(n_2+n_3)}(C_1C_2D_3D_4 - C_1C_3D_2D_4 - C_2C_4D_1D_3 + C_3C_4D_1D_2) \\ +e^{h_2(n_2+n_4)}(C_1C_4D_2D_3 - C_1C_2D_3D_4 - C_3C_4D_1D_2 + C_2C_3D_1D_4) \\ +e^{h_2(n_3+n_4)}(C_1C_3D_2D_4 - C_1C_4D_2D_3 - C_2C_3D_1D_4 + C_2C_4D_1D_3)) \\ +(e^{h_2(n_1+n_2+\beta)}(C_1D_2D_4m_3 - C_1D_2D_3m_4 - C_2D_1D_4m_3 + C_2D_1D_3m_4) \\ +e^{h_2(n_1+n_3+\beta)}(C_1D_2D_3m_4 - C_1D_3D_4m_2 - C_3D_1D_2m_4 + C_3D_1D_4m_2) \\ +e^{h_2(n_1+n_4+\beta)}(C_1D_3D_4m_2 - C_1D_2D_4m_3 - C_4D_1D_3m_2 + C_4D_1D_2m_3) \\ +e^{h_2(n_2+n_3+\beta)}(C_2D_3D_4m_1 - C_2D_1D_3m_4 - C_3D_2D_4m_1 + C_3D_1D_2m_4) \\ +e^{h_2(n_2+n_4+\beta)}(C_2D_1D_4m_3 - C_2D_3D_4m_1 - C_4D_1D_2m_3 + C_4D_2D_3m_1) \\ +e^{h_2(n_3+n_4+\beta)}(C_3D_2D_4m_1 - C_3D_1D_4m_2 - C_4D_2D_3m_1 + C_4D_1D_3m_2)) \\ (1-\kappa_2)\left(k_w + \xi^2 k_p\right) \end{bmatrix}$$

$$V_1(x_1, t_1) = \int_0^\infty \left[-\frac{(\kappa_1+1)\left(e^{4\xi h_1} + 4\xi h_1 e^{2\xi h_1} - 1\right)}{8\Delta_1\mu_1} + \frac{\kappa_1+1}{8\mu_1}\right] \sin\xi(t_1 - x_1)\, d\xi$$

$$V_2(x_1, t_2) = \int_0^\infty \left[\frac{e^{\xi h_1}(\kappa_1+1)(e^{2\xi h_1} + \xi h_1 + \xi h_1 e^{2\xi h_1} - 1)}{4\Delta_1\mu_1}\right] \sin\xi(t_2 - x_1)\, d\xi$$

15214001, 2025, 8, Downloaded from https://onlinelibrary.wiley.com/doi/10.1002/zamm.70152 by Turkey Cochrane Evidence Aid, Wiley Online Library on [07/08/2025]. See the Terms and Conditions (https://onlinelibrary.wiley.com/terms-and-conditions) on Wiley Online Library for rules of use; OA articles are governed by the applicable Creative Commons License

$$Z_1\ (x_2,\ t_1) = \int_0^\infty \left[-\frac{e^{\xi h_1}\,(\kappa_1+1)\,(e^{2\xi h_1}+\xi h_1+\xi h_1 e^{2\xi h_1}-1)}{4\Delta_1\mu_1} \right] \sin\,\xi(t_{1-}x_2)\,d\xi$$

$$Z_2\ (x_2,\ t_2) = \int_0^\infty \left[\frac{(\kappa_1+1)\left(e^{4\xi h_1}+4\xi h_1 e^{2\xi h_1}-1\right)}{8\Delta_1\mu_1} - \frac{\kappa_1+1}{8\mu_1} \right] \sin\,\xi(t_{2-}x_2)\,d\xi$$

$$Z_3\ (x_2,\ t_2) = \int_0^\infty \left[\frac{\xi}{2\Delta_2} \sum_{j=1}^{4} B_j m_j + \frac{\kappa_2+1}{8\mu_0} \right] \sin\,\xi(t_{2-}x_2)\,d\xi$$

15214001, 2025, 8, Downloaded from https://onlinelibrary.wiley.com/doi/10.1002/zamm.70152 by Turkey Cochrane Evidence Aid, Wiley Online Library on [07/08/2025]. See the Terms and Conditions (https://onlinelibrary.wiley.com/terms-and-conditions) on Wiley Online Library for rules of use; OA articles are governed by the applicable Creative Commons License